Chemical Engineering Journal 423 (2021) 130192

Contents lists available at ScienceDirect

Chemical Engineering Journal

journal homepage: www.elsevier.com/locate/cej

Phosphorylated cardanol-formaldehyde oligomers as flame-retardant and toughening agents for epoxy thermosets

Wenwen Guo [a,b], Xin Wang [a,*], Jiali Huang [a], Xiaowei Mu [a], Wei Cai [a], Lei Song [a], Yuan Hu [a,*]

[a] State Key Laboratory of Fire Science, University of Science and Technology of China, 96 Jinzhai Road, Hefei, Anhui 230026, PR China
[b] Key Laboratory of Eco-textiles, Ministry of Education, College of Textile Science and Engineering, Jiangnan University, 1800 Lihu Avenue, Wuxi, Jiangsu 214122, PR China

ARTICLE INFO

Keywords:
Cardanol
Epoxy thermoset
Flame-retardant
Toughening

ABSTRACT

Presently, flammability and brittleness are two major problems for EP which has restricted its development and application in industrial. Under the global advocacy of green and sustainable development, developing bio-based flame-retardant and toughening agents which can endow epoxy resins with high fire resistance and satisfactory mechanical properties is of significant demand for its industrial applications. Herein, three kinds of phosphorylated cardanol-formaldehyde oligomers (CF-PO(OPh)$_2$, CF-POPh$_2$, and CF-PPh$_2$) were synthesized and introduced into epoxy thermosets. The incorporation of CF-PO(OPh)$_2$, CF-POPh$_2$, and CF-PPh$_2$ can remarkably improve the mechanical performance of EP composites, especially the tensile strength and elongation at break. With 10 wt% of CF-PO(OPh)$_2$, CF-POPh$_2$, and CF-PPh$_2$, the tensile strength of epoxy thermosets reached 67.1, 74.5, and 70.3 MPa, respectively; the elongation at break of epoxy thermosets was raised by 133.3%, 162.5%, and 150.0%, respectively, as compared to neat EP. EP composites containing CF-PO(OPh)$_2$, CF-POPh$_2$, and CF-PPh$_2$ also exhibited remarkably enhanced flame retardancy simultaneously. Besides, CF-PO(OPh)$_2$ exhibited the best flame-retardant efficiency by comparison with CF-POPh$_2$ and CF-PPh$_2$, and the results manifested that epoxy composite with only 2.5 wt% CF-PO(OPh)$_2$ could pass the UL-94 V-0 rating as well as a high LOI value of 28%, and the LOI value of EP/CF-PO(OPh)$_2$–10 reached up to 32%. Moreover, CF-PO(OPh)$_2$ also displayed an excellent catalytic charring effect and great suppression effect on heat and smoke release. The cone calorimeter test results showed that EP composite containing 10 wt% CF-PO(OPh)$_2$ exhibited the most significant PHRR reduction which was 53.8% lower than pure EP, and the char yield of EP/CF-PO(OPh)$_2$–10 after the cone calorimeter test was 14.0% which was much higher than that of pure EP (5.7%). This work opens a new vision for the synthesis of bio-based flame-retardant and toughening agents with a special oligomeric structure combining rigidity with flexibility, and contributes to the production of high-performance epoxy thermosets.

1. Introduction

Epoxy resin (EP), as a prominent class of generally accepted commercially thermosetting resins, has an extensive demand in the fields of adhesives, coatings, insulation materials, electronics as well as high-performance composites own to its excellent comprehensive performance including high mechanical strength, good chemical resistance, exceptional adhesion ability and superior electrical insulation property [1–3]. Unfortunately, epoxy resin usually behaves undesirably brittleness with poor impact resistance ascribed to the high cross-linking density of its backbone structure [4,5], which severely restricts its applications in the engineering fields of high-performance materials that

Abbreviations: EP, Epoxy resin; DGEBA, Bisphenol A epoxy resin; CFR, Cardanol-formaldehyde resin; PO(OPh)$_2$Cl, Diphenyl phosphoryl chloride; POPh$_2$Cl, Diphenylphosphinic chloride; PPh$_2$Cl, Chlorodiphenylphosphine; CF-PO(OPh)$_2$, CF-POPh$_2$, CF-PPh$_2$, three kinds of phosphorylated cardanol-formaldehyde oligomers; DDM, 4,4′-diamino-diphenylmethane; TEA, Triethylamine; DMF, N, n-dimethylformamide; NMR, Nuclear magnetic resonance spectroscopy; FTIR, Fourier transform infrared spectroscopy; GPC, Gel permeation chromatography; DSC, Differential scanning calorimetry; TGA, Thermogravimetric analysis; UL-94, Vertical burning test; LOI, Limiting oxygen index; SEM, Scanning electron microscope; $T_{-10\%}$, the temperature at 10 wt% mass loss; T_{-75}, the temperature at 75 wt% mass loss; T_{max}, the temperature at the maximum mass loss rate; T_g, Glass transition temperature; TTI, Time to ignition; T_{PHRR}, Time to PHRR; HRR, Heat release rate; THR, Total heat release; SPR, Smoke production rate; FIGRA, Fire spread rate index.

* Corresponding author.
E-mail addresses: wxcmx@ustc.edu.cn (X. Wang), yuanhu@ustc.edu.cn (Y. Hu).

https://doi.org/10.1016/j.cej.2021.130192
Received 20 November 2020; Received in revised form 29 April 2021; Accepted 2 May 2021
Available online 4 May 2021

require outstanding toughness to prevent easy fractures and damages during the long-term daily applications [6].

To improve the impact resistance, considerable efforts have been made to the toughening modification of epoxy resins. At present, the popular strategy to toughen epoxy resins is mainly through incorporating inorganic nanoparticles such as silica [7], graphene [8,9], molybdenum disulfide [10], and nanofibers [11] or organic materials including thermoplastic polymers [12], rubber [13] and compounds containing flexible segments [14] into EP matrix. It has been reported that the former modification method of nanoparticles can make great contributions to the improvement of impact resistance of EP composites via promoting the formation of stress whitening and shear band at the interface, which can efficiently dissipate the impact energy and decrease the stress concentration inside the matrix, thereby inhibiting the initiation and propagation of crack [15,16]. Nevertheless, the enhancement in impact toughness is generally accompanied by the processing difficulty caused by the increased viscosity of the epoxy matrix, meanwhile, the dispersion of nanoparticles in the EP matrix is another challenging problem that makes it difficult for nanoparticles to achieve the same magnitude in the enhancement of impact strength as organic flexible reinforcements [6]. The introduction of organic toughening agents into EP matrix exhibits great compatibility and brings excellent enhancements in impact resistance, which is thereby considered the more effective toughening technique for epoxy resins.

However, the commonly used organic toughening materials are generally derived from petroleum resources. In recent years, the increasing depletion of petroleum resources and rising environmental pollution appear to be two major challenges for society in the 21st century [17,18]. In this regard, developing the bio-based sustainable feedstock into environment-friendly chemicals and products via a clean and convenient method to replace the petroleum-based raw materials possesses broad application prospects to alleviate energy and environmental pressure. So far, extensive publications have frequently reported synthesizing green and sustainable toughening/reinforcing agents from renewable bio-based raw materials [4,19–21]. Chu *et al.* synthesized a renewable vanillin-based flame retardant toughening agent (PVSi) [6]. EP thermosets with PVSi presented enhanced fire safety performance accompanied by excellent impact toughness attributed to the polar phosphaphenanthrene and flexible phenylsiloxane groups. Qi *et al.* has constructed a bio-based epoxy precursor (THMT-EP) by using an aromatic triazine derivative from vanillin [22], and the cured THMT-EP exhibited remarkable integrated properties including a high flexural modulus of 4137 MPa as well as a flexural strength of 134.2 MPa, which were 53.9% and 14.3% higher than those of commercial DGEBA, respectively. Xiao *et al.* synthesized a renewable toughening agent (TAA) by introducing cyano groups into tung oil [14]. Epoxy resins containing TAA displayed a significant enhancement of toughness, specifically, impact strength, toughness, and elongation at break were capable to reach 76.7 kJ/m^2, 7.6 MJ/m^3, and 25.0%, respectively (pure epoxy resin: 21.1 kJ/m^2, 3.1 MJ/m^3, and 5.7%). These results above demonstrated that bio-based toughing agents can significantly improve the mechanical toughness which caught more and more attention in the fields of toughening epoxy resins. Among various biomass resources, cardanol is an inexpensive, easily available, and eco-friendly agricultural byproduct extracted from cashew nut shell liquid. It has a unique chemical structure with both rigid aromatic rings and flexible long aliphatic chains which would afford an exceptional combination of mechanical strength and toughness, indicating that cardanol can be an excellent candidate in the applications of toughening epoxy thermosets [23–26]. Additionally, the phenolic hydroxyl and unsaturated double bond in the structure of cardanol afford a versatile platform for diverse chemical modification [27], which not only makes it possible for the generation of various cardanol-derived toughening agents, but also can endow a series of new functions to cardanol-based derivatives through multifunctional chemical modification.

Besides the intrinsic drawback of mechanical brittleness, the high flammability of epoxy thermoset is another fatal defect that severely restricts its applications in the field of electronic devices, coating, and composites which required high flame retardancy [28,29]. Therefore, it is imperative to construct high available, low-cost, and eco-friendly biomass-derived products which possess excellent flame retardancy as well as toughness. Recently, a few cardanol-based flame-retardant and toughening agents have been developed to simultaneously enhance the flame retardancy and toughness of epoxy resins [2,5], but high loading of these cardanol-based agents is required to achieve a satisfactory flame-retardant and toughening effect. Moreover, these cardanol-derived flame-retardant and toughening agents are small-molecular products, the oligomeric flame-retardant and toughening agents have been rarely reported.

In an attempt to simultaneously impart flame retardancy and toughness to epoxy resins, three kinds of phosphorylated cardanol-formaldehyde oligomers (CF-PO(OPh)$_2$, CF-POPh$_2$, and CF-PPh$_2$) were synthesized. The chemical structures of CF-PO(OPh)$_2$, CF-POPh$_2$, and CF-PPh$_2$ were confirmed through nuclear magnetic resonance (NMR) and Fourier transform infrared spectroscopy (FTIR). To investigate the influence of the types and amounts of phosphorylated cardanol-formaldehyde oligomers on flame retardancy and toughness of epoxy resins, a series of EP composites with different contents of CF-PO(OPh)$_2$, CF-POPh$_2$, and CF-PPh$_2$ were prepared by utilizing 4,4-diaminodiphenyl methane (DDM) as a curing agent. The curing behavior, thermal, mechanical, and fire retardant performances of EP composites with different contents of CF-PO(OPh)$_2$, CF-POPh$_2$, and CF-PPh$_2$ were evaluated by DSC, TGA, tensile and impact test, UL-94, LOI, and cone calorimeter tests. Additionally, the flame-retardant mechanism of phosphorylated cardanol-formaldehyde oligomers was also studied.

2. Experimental section

2.1. Chemicals

Cardanol was supplied by Cardolite Corporation (Zhuhai, China). Bisphenol A-type epoxy resin (DGEBA, commercial brand: E-44, EEW: 227 g/equivalent) was obtained from Hefei Jiangfeng Chemical Industry Co. Ltd (Anhui, China). Diphenyl phosphoryl chloride (PO(OPh)$_2$Cl), diphenylphosphinic chloride (POPh$_2$Cl), chlorodiphenylphosphine (PPh$_2$Cl), anhydrous magnesium sulfate, and ammonia were purchased from Aladdin Industrial Corporation (Shanghai, China). 4,4′-diaminodiphenylmethane (DDM), triethylamine (TEA), aqueous formaldehyde (37%), acetone, and chloroform were purchased from Sinopharm Chemical Reagent Co. Ltd. (Shanghai, China). All the reagents were used as received without further purification.

2.2. Synthesis of cardanol-formaldehyde resin (CFR)

Cardanol-formaldehyde resin (CFR) was synthesized by cardanol and formaldehyde with a molar ratio of 1:0.7 using ammonia as the catalyst according to the previous reports [30]. Briefly, cardanol (0.1 mol), and ammonia (1 wt% of cardanol) were introduced into a 1L three-necked and round-bottomed flask equipped with a condenser, mechanical stirrer, and thermometer. Then, formaldehyde (37%, 0.07 mol) was added to the solution through a dropping funnel under stirring. The reaction was carried out at 85 ℃ for 3 h. Subsequently, the obtained viscous liquid was further evaporated under a vacuum to remove the remaining water and ammonia, yielding a brown liquid product (Yield: 91.5%). The schematic diagram of the synthetic process of CFR is illustrated in Scheme 1.

2.3. Synthesis of phosphorylated cardanol-formaldehyde oligomers

Phosphorylated cardanol-formaldehyde oligomers were fabricated according to the previous literature [5]. In detail, CFR (0.30 mol) and triethylamine (0.30 mol) were dissolved in dry chloroform (200 mL) in a

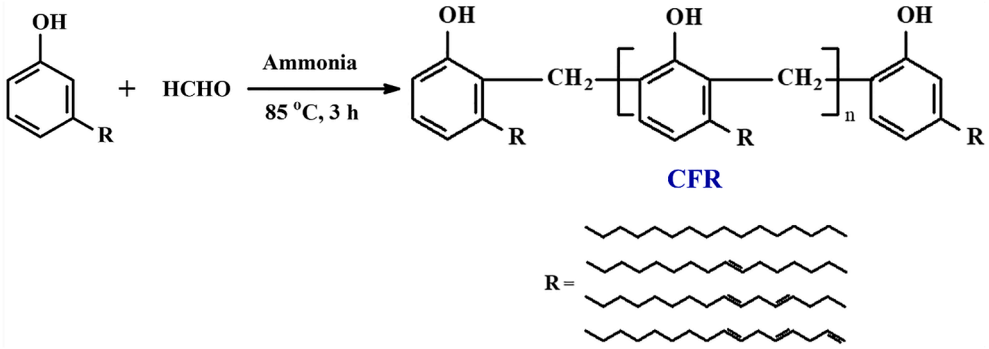

Scheme 1. Schematic diagram of the synthetic process of CFR.

three-necked round-bottomed flask equipped with a magnetic stirrer and a reflux condenser. Furthermore, diphenyl phosphoryl chloride (0.30 mol) was introduced dropwise into the system at 0 °C. The reaction was then conducted at 60 °C for 6 h. After cooling down to room temperature, the solution was filtered to remove the white precipitate, and the filtrate was further washed with deionized water three times. The organic layer was dried with anhydrous magnesium sulfate and the solvent was removed under reduced pressure. The brown viscous product was CF-PO(OPh)$_2$ (Yield: 82.9%). The reaction completion was checked by thin-layer chromatography (Fig. S1). Similarly, CF-POPh$_2$ (Yield: 84.3%) and CF-PPh$_2$ (Yield: 81.5%) were synthesized by the same procedure, just replacing diphenyl phosphoryl chloride with diphenylphosphinic chloride and chlorodiphenylphosphine, respectively. Because CF-PPh$_2$ was prone to be oxidized slowly in the air, it was stored in a bottle filled with nitrogen. The CF-PPh$_2$ should be used instantly after being taken out from the stored bottle. The synthetic route of three kinds of phosphorylated cardanol-formaldehyde oligomers (CF-PO(OPh)$_2$, CF-POPh$_2$, and CF-PPh$_2$) are illustrated in Scheme 2.

2.4. Preparation of EP and its composites

A series of EP/CF-PO(OPh)$_2$, EP/CF-POPh$_2$, and EP/CF-PPh$_2$ composites with different contents of additives were prepared, and the formulations are summarized in Table 1. Taking EP/CF-PO(OPh)$_2$–2.5 composite as an example, the preparation procedure was depicted as follows: typically, DGEBA was firstly mixed with 2.5 wt% CF-PO(OPh)$_2$ adequately under stirring at 100 °C for 30 min. Then, DDM was mixed into the above mixture for 2–3 min. Subsequently, the mixture was cured at 100 °C for 2 h and post-cured at 150 °C for 2 h. Finally, the

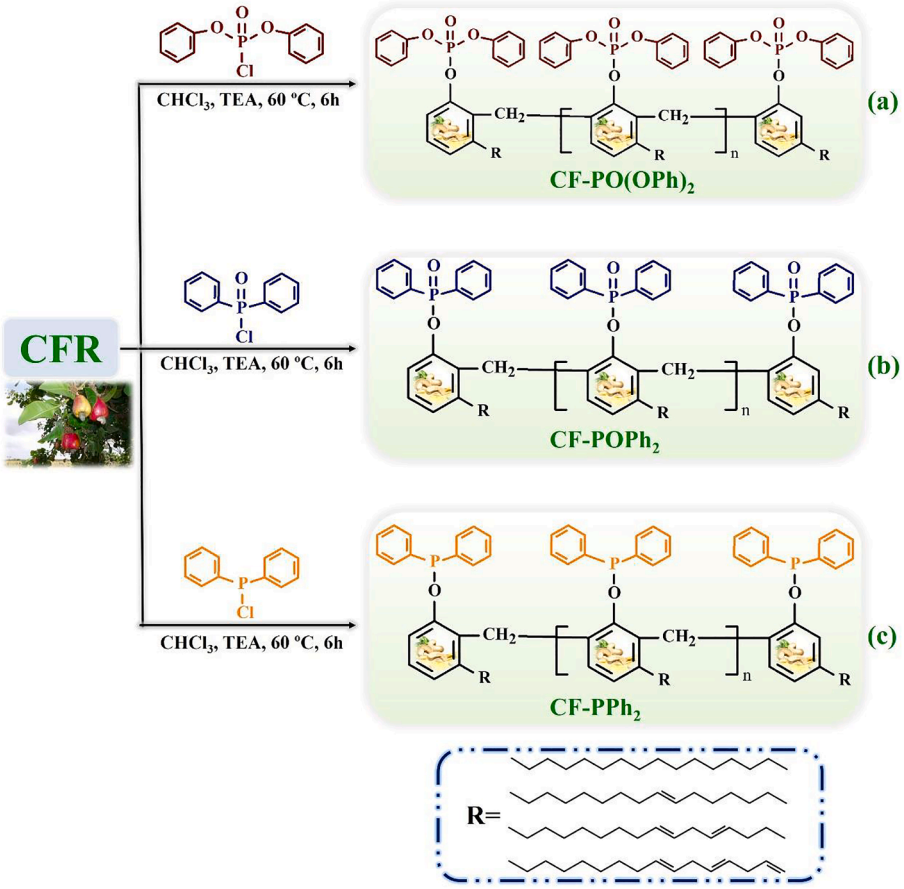

Scheme 2. Synthetic route of three kinds of phosphorylated cardanol-formaldehyde oligomers: (a) CF-PO(OPh)$_2$, (b) CF-POPh$_2$, and (c) CF-PPh$_2$.

Table 1
Formulations of EP and its composites.

Sample	EP (wt %)	CF-PO(OPh)$_2$ (wt%)	CF-POPh$_2$ (wt %)	CF-PPh$_2$ (wt %)
EP	100	0	0	0
EP/CF-PO (OPh)$_2$–2.5	97.5	2.5	0	0
EP/CF-PO (OPh)$_2$–5	95	5	0	0
EP/CF-PO (OPh)$_2$–10	90	10	0	0
EP/CF-POPh$_2$-2.5	97.5	0	2.5	0
EP/CF-POPh$_2$-5	95	0	5	0
EP/CF-POPh$_2$-10	90	0	10	0
EP/CF-PPh$_2$-2.5	97.5	0	0	2.5
EP/CF-PPh$_2$-5	95	0	0	5
EP/CF-PPh$_2$-10	90	0	0	10

cured samples were cooled down to room temperature. Pure EP and other EP composites with different contents of CF-PO(OPh)$_2$, CF-POPh$_2$, and CF-PPh$_2$ were prepared through a similar procedure.

2.5. Characterization

Nuclear magnetic resonance analysis (NMR), Fourier transform infrared (FTIR) and gel permeation chromatography (GPC) were employed to characterize the structure of the synthesized products. ^{1}H NMR, ^{13}C NMR, and ^{31}P NMR spectra of samples were performed on an AV400 Bruker spectrometer (Bruker BioSpin, Switzerland) by utilizing deuterated chloroform ($CDCl_3$) as the solvent; FTIR spectra were recorded on a Nicolet 6700 spectrometer (Nicolet Instrument Co., USA); GPC was carried out on an instrument equipped with a G1310B ISO pump, a G1316A PLgel column, and a G1362A differential refractive index detector. The eluent was N, N-dimethylformamide (DMF) with 1.0 g/L LiBr with a flow rate of 1.0 mL/min. A series of low-polydispersity polystyrene standards were applied for calibration. The carbon and oxygen elemental analysis was determined by a Vario EL cube element analyzer (Elementar, Germany). The phosphorus content was determined by an Opmita 7300 DV inductively coupled plasma optic emission spectrometer (PerkinElmer, USA).

Differential scanning calorimetry (DSC) was performed on a DSC Q2000 (TA Instruments Inc., USA) under nitrogen. To study the curing behaviors of EP and its composites, a small amount of uncured mixtures (7–10 mg) was subjected into DSC cell and heated from 30 °C to 300 °C with different heating rates (5, 10, 15 and 20 °C/min) under nitrogen atmosphere. To measure the glass transition temperature (T_g), EP and its composites were tested at a heating rate of 10 °C/min.

Thermogravimetric analysis (TGA) was conducted on a Q5000 thermal analyzer (TA Co., USA) under both air and nitrogen atmospheres with a heating rate of 20 °C/min.

The mechanical properties of EP and its composites were studied by tensile and impact tests. The tensile tests were carried out on criterion 43 universal testing machine (MTS, USA) according to the ASTM D3039-08 method, and the test for each sample was repeated for at least five runs with a speed of 2 mm/min. The Charpy impact test of the samples without notch was performed on a ZBC1400-A pendulum impact testing machine (MTS Systems, China) following the GB/T 1043.1–2008 standard, and at least five runs were repeated for each sample (80 mm × 10 mm × 4 mm) under impact energy of 4 J.

Limiting oxygen index (LOI), vertical burning test (UL-94), and cone calorimeter tests were employed to measure the flame retardancy of EP and its composites. LOI measurement was conducted on an HC-2 oxygen index meter according to ASTM D2863-2010 standard, and the dimension of specimens was 100 × 6.5 × 3.0 mm^3; UL-94 tests were conducted on a CFZ-2 type instrument referring to the ASTM D3801-1996 standard and the samples were in the dimension of 130.0 × 13.0 × 3.2 mm^3; EP and its composites were also subjected to cone calorimeter following the ASTM E1354/ISO 5660, the size of specimens is 100 × 100 × 3 mm^3 while the heat flux is 50 kW/m^2.

The microstructures of char residues of EP and its composites after cone calorimeter tests were investigated on a JEOL JSM-6700 scanning electron microscope (SEM) and a LabRAM-HR Confocal Raman Microprobe applying a 514.5 nm argon-ion laser.

3. Results and discussion

3.1. Structural characterization

To verify the successful synthesis of CFR, CF-PO(OPh)$_2$, CF-POPh$_2$, and CF-PPh$_2$, the NMR measurements were employed to study the structures of the products. In the ^{1}H NMR spectrum of CFR (Fig. 1a), the peaks at 7.11, 6.74, and 6.63 ppm are attributed to the protons (b, c and a, d) of the benzene ring. The peaks at 5.82 ppm (k) and 5.01 ppm (l) are assigned to the terminal vinyl protons of the triene moiety. The peak at 5.36 ppm is due to the double-bond protons (i) of the monoene, diene, and triene moieties. The signals in the range of 0.8–2.8 ppm are ascribed to the methylene groups, whereas the allylic protons (h) of the monoene, diene, and triene moieties resonated at 2.03 ppm, the strong signal at around 1.32 ppm is ascribed to the long aliphatic chains and the peak at 0.88 ppm is the terminal methyl groups of pentadecyl, monoene and diene moieties [5]. Moreover, the protons of the methylene units bridging to phenyl groups can be observed at around 2.03 ppm [30]. Fig. 1b shows the ^{13}C NMR spectrum of CFR. The feature of novolac resin can be verified by the resonance related to the bridging methylene carbons, which can be evidenced by the appearance of ortho–ortho bridge carbon observed at 30.4 ppm, and it is also in good agreement with the previous report [30]. Additionally, the signal at 155.63 ppm is ascribed to the aromatic carbon attached to the oxygen atom (Ph − OH, a), and the chemical shift of the carbons at 144.82 ppm results from the aromatic carbon of Ph-R$_1$ (b). The unsaturated carbon atoms originate from the benzene ring and the side chain can be observed in the range of 137.0–112.3 ppm, while the signals at 36.0–13.97 ppm are assigned to the methylene carbons originates from the long aliphatic side chains. Moreover, the signal observed at 77.19 ppm is due to the deuterated chloroform. All these data from ^{1}H NMR and ^{13}C NMR indicate the successful synthesis of CFR. The ^{1}H NMR pattern of CF-PO(OPh)$_2$ (Fig. 1c) is very similar to that of CFR, but the aromatic protons (7.35–7.03 ppm) show a different chemical shift as compared to that of CFR (7.11–6.63 ppm), which is due to the substitution of -PO(OPh)$_2$ group. The ^{1}H NMR spectrum of diphenyl phosphoryl chloride (Fig. S2a) shows a similar chemical shift of the protons of benzene ring as that of CF-PO(OPh)$_2$, which indicates the successful substitution reaction between CFR and diphenyl phosphoryl chloride. Additionally, the ^{31}P NMR spectrum of diphenyl phosphoryl chloride exhibits a single signal at −5.09 ppm (Fig. S2b), which shifts to −17.78 ppm in the ^{31}P NMR spectrum of CF-PO(OPh)$_2$ (Fig. 1d) after the reaction of PO(OPh)$_2$Cl and CFR. These results are well consistent with the expected chemical structure of CF-PO(OPh)$_2$, implying the successful substitution reaction between PO(OPh)$_2$Cl and CFR. Analogously, similar results can be observed in the ^{1}H NMR and ^{31}P NMR spectra of CF-POPh$_2$ and CF-PPh$_2$, respectively. The ^{1}H NMR of both CF-POPh$_2$ (Fig. 1e) and CF-PPh$_2$ (Fig. 1g) display a similar pattern as that of CFR, except for a different chemical shift of their aromatic protons' peaks. Moreover, there is a single peak in the ^{31}P NMR spectra for both CF-POPh$_2$ (Fig. 1f) and CF-PPh$_2$ (Fig. 1h), and the chemical shift is 29.86 and 21.41 ppm, respectively. By comparison, the chemical shift in the ^{31}P NMR spectra of POPh$_2$ (Fig. S2c) and CF-PPh$_2$ (Fig. S2d) is 44.50 and 81.54 ppm, respectively. All these results indicate the successful synthesis of CF-POPh$_2$ and CF-PPh$_2$.

To further prove the chemical structure of the products, FTIR spectroscopy was also measured, and the spectra are shown in Fig. 2. In the FTIR spectrum of CFR, the broad peaks at 3404 and 1347 cm^{-1} are assigned to the stretching vibration of phenol hydroxyl [31,32]. The

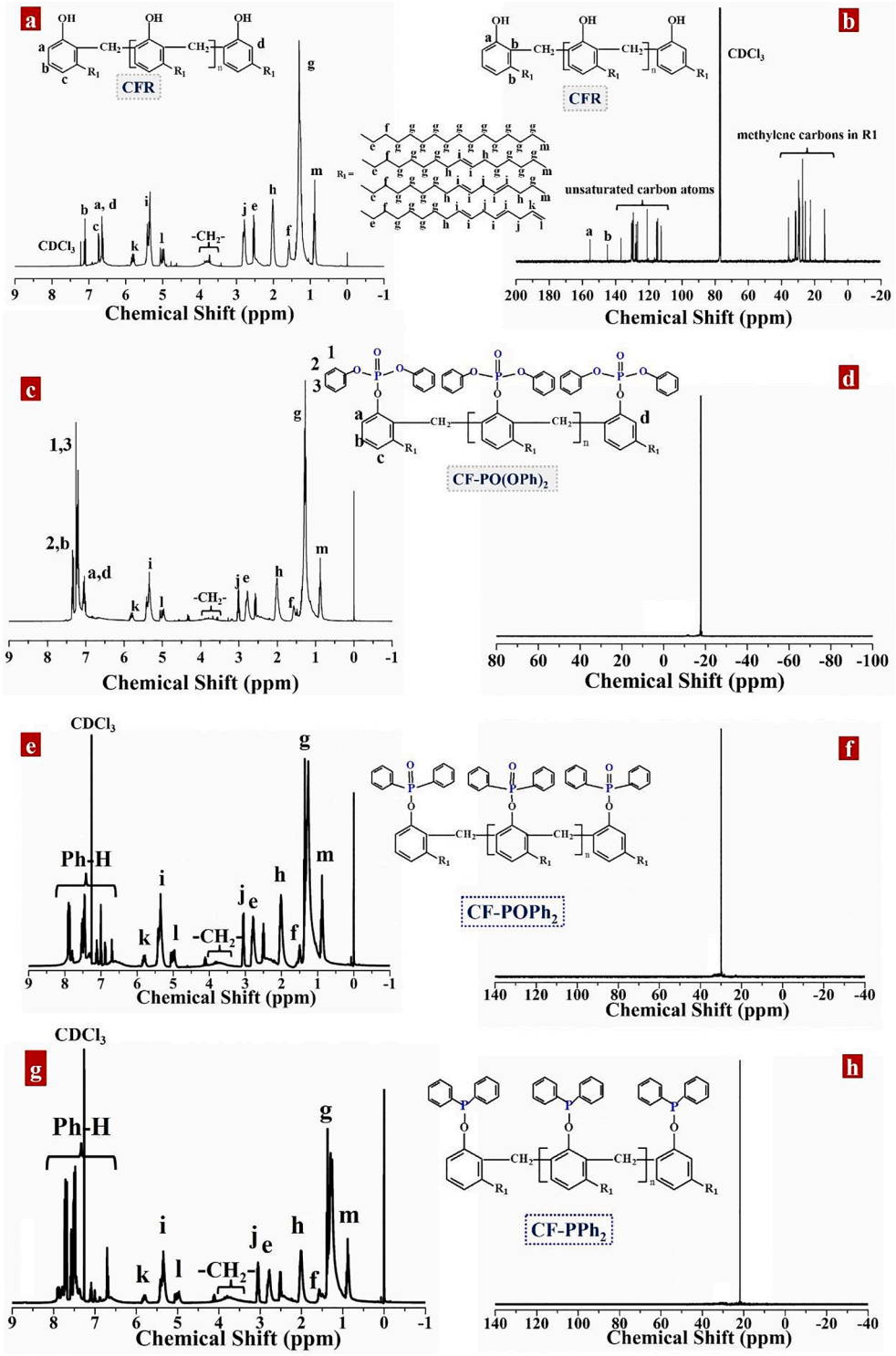

Fig. 1. (a) ^{1}H NMR and (b) ^{13}C NMR spectra of CFR, ^{1}H NMR and ^{31}P NMR spectra (c, d) CF-PO(OPh)$_2$, (e, f) CF-POPh$_2$, and (g, h) CF-PPh$_2$.

absorption peak at 3008 cm^{-1} is ascribed to the unsaturated double bonds (C = C) stretching of the long aliphatic side chains. The signals located at 2922 cm^{-1}and 2850 cm^{-1} are attributed to the antisymmetric and symmetric stretching vibration of –CH_3 and –CH_2 groups, respectively. The peaks at 1589 cm^{-1}and 1459 cm^{-1} are owing to the skeleton deformation vibrations of the aromatic ring [33]. The bands located at 1263 and 1153 cm^{-1} belong to the stretching vibration of C-O, which is between phenolic hydroxyl and benzene ring groups [33]. The appearance of the peak at 986 cm^{-1} indicates the ortho substitution of CH_2OH, which demonstrates the methylation of cardanol [34,35]. The signals at 776 and 697 cm^{-1} correspond to the bending vibrations of C–H adjacent to the benzene ring, which implies that the benzene ring is *meta*-substituted with phenolic hydroxyl and alkyl chains [33]. The FTIR spectrum of PO(OPh)$_2$Cl (Fig. 2a) presents several characteristic groups, such as P = O (1173 cm^{-1}), P-O-Ph (958–1130 cm^{-1}), and P-Cl (542–587 cm^{-1}), After the substitution reaction between CFR and PO(OPh)$_2$Cl, the P-Cl peak disappears and other characteristic peaks of PO(OPh)$_2$Cl can be observed in the FTIR spectrum of CF-PO(OPh)$_2$

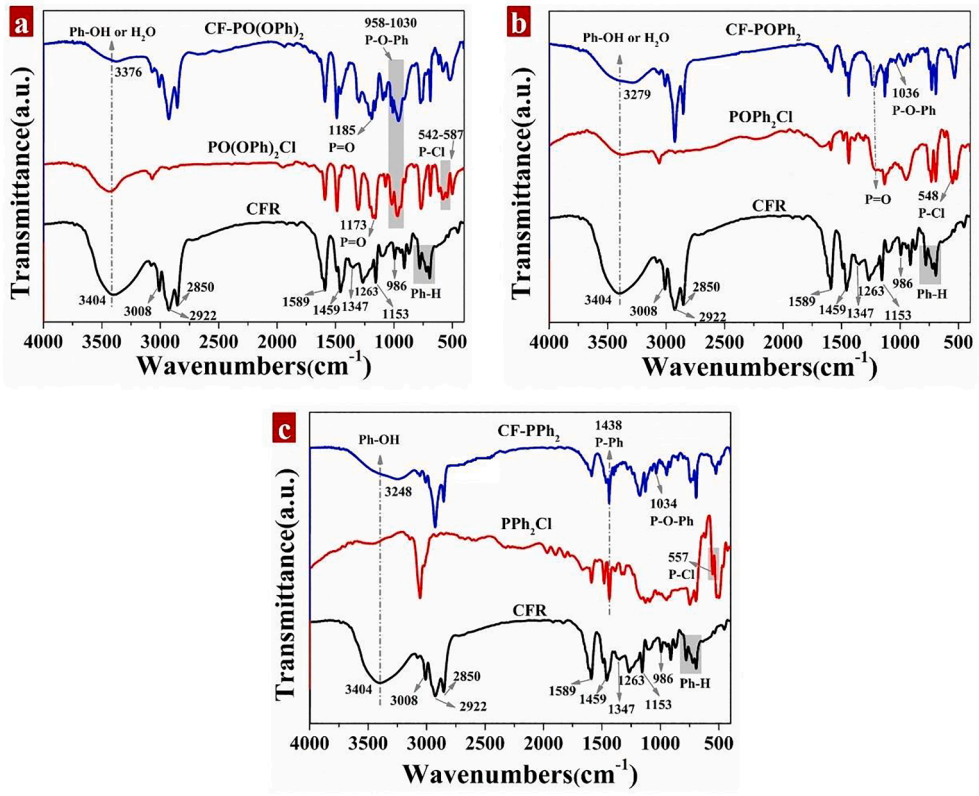

Fig. 2. FTIR spectra of (a-c) CFR, (a) CF-PO(OPh)$_2$, (b) CF-POPh$_2$ and (c) CF-PPh$_2$.

(Fig. 2a). Moreover, compared to the spectrum of CFR, the signal at 1347 cm^{-1} disappears, the strong broad peak of the phenolic hydroxyl group shifts from 3404 to 3376 cm^{-1}, and the intensity of the signal weakens. The results confirmed that the successful synthesis of CF-PO(OPh)$_2$. In the case of CF-POPh$_2$ (Fig. 2b) and CF-PPh$_2$ (Fig. 2c), similar results can be concluded from their FTIR spectra. Additionally, the new peak of P-O-Ph appears in the FTIR spectra of CF-POPh$_2$ and CF-PPh$_2$ at 1036 and 1034 cm^{-1}, respectively, demonstrating the successful synthesis of CF-POPh$_2$ and CF-PPh$_2$.

The molecular weight of CFR, CF-PO(OPh)$_2$, CF-POPh$_2$, and CF-PPh$_2$ is determined by GPC, as summarized in Table S1. The number average molecular weight (M_n) of CFR is 1679 g/mol with the polydispersity index (PDI) of 1.23, demonstrating the oligomeric structure of CFR [36]. After phosphorylation, CF-PO(OPh)$_2$ (M_n: 2204 g/mol, PDI: 2.01), CF-POPh$_2$ (M_n: 2160 g/mol, PDI: 1.87), and CF-PPh$_2$ (M_n: 2089 g/mol, PDI: 1.96) exhibit larger M_n and PDI than those of CFR, implying that the phosphorus-containing structure has been successfully bonded to cardanol-formaldehyde resin. The elemental analysis results of CF-PO(OPh)$_2$, CF-POPh$_2$, and CF-PPh$_2$ are listed in Table S2. It can be found that the measured values of carbon, oxygen, and phosphorus contents correspond well with the theoretical ones, implying the successful synthesis of the target products with high purity.

3.2. Curing behavior of EP and its composites

The cure kinetics of EP and its composites were investigated using DSC analysis. The information about the theoretical background is given in the supporting information in detail. The non-isothermal DSC tests were conducted under multiple heating rate scans (5, 10, 15, and 20 °C/min) and the corresponding curves are shown in Fig. S3. The characteristic temperatures such as the initial curing temperature (T_{onset}), the peak curing temperature (T_p), and the final curing temperature (T_{end}) of EP curing systems can be obtained from the DSC curves, and the relevant results are summarized in Table S3. According to the equation (S1), the relationship between the extent of conversion (α) and temperature could be obtained by integrating the DSC curve, as shown in Fig. S4. The curing process conditions of a specific curing system can be preliminarily estimated according to the relationship between the curing characteristic temperature (T_{onset}, T_p, and T_{end}) and β for each curing system. Fig. S5 presents the linear fitting plot of T_{onset}, T_p, and T_{end} versus β of each curing system. The characteristic curing temperature can be acquired by extrapolating the fitting curves (β = 0) as summarized in Table S4.

According to Kissinger's and Ozawa's equations, the linear fitting plots of $\ln(\beta/T_p^2)$-$1/T_p$ and $\ln\beta$-$1/T_p$ are depicted in Fig. 3a and Fig. 3b, respectively. The E_as calculated by Kissinger's and Ozawa's methods and the reaction order (n) obtained according to Crane's equation is listed in Table S4. As depicted in Fig. 3, the data points of $\ln(\beta/T_p^2)$-$1/T_p$ and $\ln\beta$-$1/T_p$ for all curing systems have a good linear correlation. Although the E_as calculated by Ozawa's method are slightly higher than those acquired by Kissinger's method, the overall changing trend of E_as calculated by the two methods is the same. Moreover, all the E_a values of six curing systems are between 47 and 65 kJ/mol, which is within the range of the reported values for epoxy-amine curing systems, manifesting that the fitting results are reliable. Taking E_a calculated by Kissinger's method as an example, the E_a of pure EP is 47.59 kJ/mol. After modification, the E_a of EP/CF-PO(OPh)$_2$–2.5 is enhanced to 51.27 kJ/mol. With increasing the amount of CF-PO(OPh)$_2$ in the curing system, the E_a value gradually increases, which is mainly caused by three factors: Firstly, the apparent viscosity of CF-PO(OPh)$_2$ is higher than that of epoxy resin. The incorporation of CF-PO(OPh)$_2$ into epoxy matrix could increase the viscosity of the system, thereby hindering the molecular movement of epoxy and curing agent; Secondly, CF-PO(OPh)$_2$ possesses a large number of aromatic rings, and the steric hindrance effect could cause the increased E_a [37]. Thirdly, the P = O structure in CF-PO(OPh)$_2$ is a strong electron-withdrawing group, which could reduce the electron cloud density of the curing agent to obstruct the nucleophilic substitution reaction between amino and epoxy groups [37]. Similarly, CF-

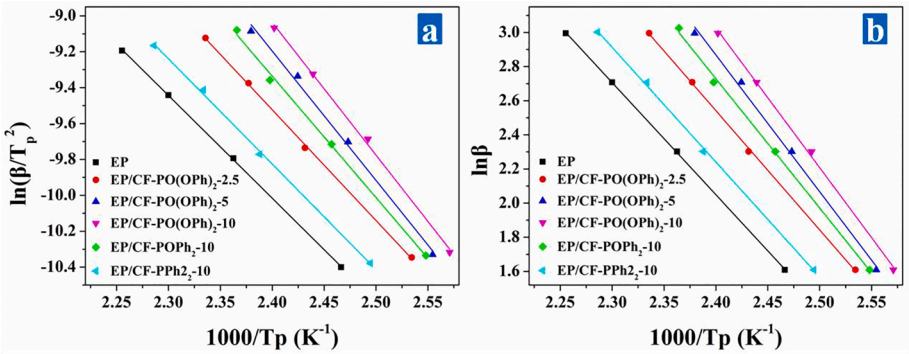

Fig. 3. The linear fitting plots of (a) $\ln(\beta/T_p^2)$-$1/T_p$ and (b) $\ln\beta$-$1/T_p$ of EP and its composites according to Kissinger's and Ozawa's equations, respectively.

$POPh_2$ has a hindering effect on the curing process of EP composites, and the E_a of EP/CF-$POPh_2$-10 is 56.22 kJ/mol. Notably, CF-PPh_2 has no significant influence on E_a as compared to CF-$PO(OPh)_2$ and CF-$POPh_2$, because there is no strong electron-withdrawing group in its structure. Thereby, the hindering effect of CF-PPh_2 on the curing reaction is weaker than that of the other two cardanol-derived oligomers. Besides, the incorporation of CF-$PO(OPh)_2$, CF-$POPh_2$, and CF-PPh_2 has a slight effect on the reaction order (n) and n of all the curing systems is approximately 0.92, which is a first-order reaction. These results indicate that the incorporation of three kinds of phosphorylated cardanol-formaldehyde oligomers into the EP matrix does not show obvious effects on the curing reaction.

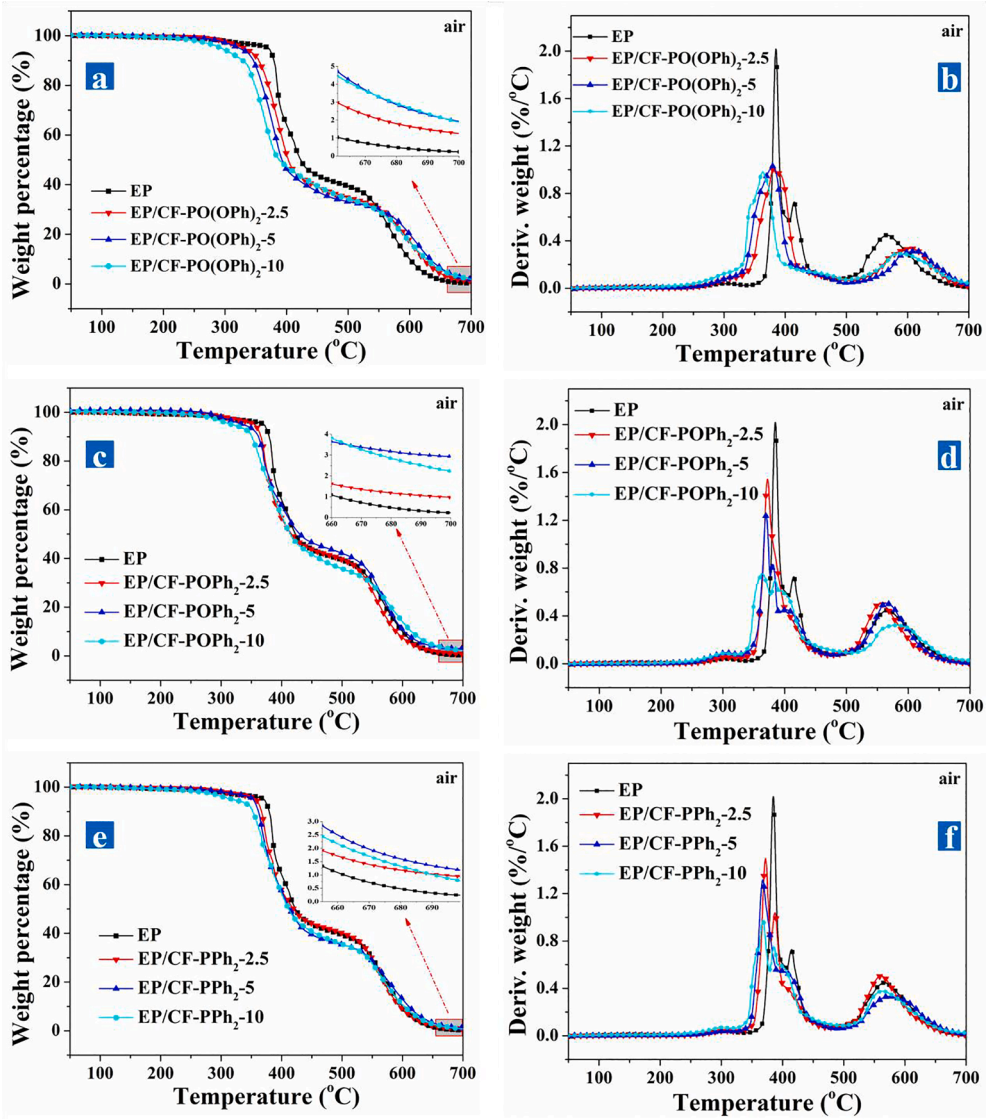

Fig. 4. TGA and DTG curves of (a, b) EP/CF-$PO(OPh)_2$, (c, d) EP/CF-$POPh_2$, and (e, f) EP/CF-PPh_2 composites under air atmosphere.

3.3. Thermal performances of EP and its composites

The influence of CF-PO(OPh)$_2$, CF-POPh$_2$, and CF-PPh$_2$ on the thermal degradation process of epoxy composites was evaluated by TGA under both air and nitrogen atmosphere. Several typical temperatures such as $T_{-5\%}$ (the temperature at 5 wt% mass loss), $T_{-10\%}$ (the temperature at 10 wt% mass loss), $T_{-30\%}$ (the temperature at 30 wt% mass loss), and T_{max} (the temperature corresponding to the maximum mass loss rate) are summarized in Table S5. As illustrated in Fig. 4a, under air atmosphere, the thermal-oxidative degradation process of pristine EP could be chiefly divided into two stages: the first stage corresponds to the thermal degradation caused by the fracture of the epoxy resin cross-linking network (355–470 °C, approximately 55 wt% weight loss); the second stage (480–650 °C, about 42 wt% weight loss) is mainly the process of further thermal oxidative degradation of the formed unstable char layer [2,38,39]. The thermal oxidative degradation behaviors of EP/CF-PO(OPh)$_2$, EP/CF-POPh$_2$, and EP/CF-PPh$_2$ composites are very similar to that of EP. Whereas, the $T_{-10\%}$ and T_{max1} of the composites present varying degrees of reduction as compared to pure EP. Taking EP/CF-PO(OPh)$_2$ composites as an instance, the $T_{-10\%}$ and T_{max1} of pure EP are 379.1 and 384.7 °C, respectively. After the introduction of CF-PO(OPh)$_2$, the $T_{-10\%}$ and T_{max1} of EP/CF-PO(OPh)$_2$–2.5 reduce to 355.0 and 383.4 °C, respectively. With further augmenting the addition CF-PO(OPh)$_2$, the $T_{-10\%}$ and T_{max1} of EP/CF-PO(OPh)$_2$–5 and EP/CF-PO(OPh)$_2$–10 are further decreased, which are mainly ascribed to the early degradation of CF-PO(OPh)$_2$ in the EP composites. In the initial heating stage, CF-PO(OPh)$_2$ with phosphate structure decomposes in advance to produce polyphosphoric acid or metaphosphoric acid which possesses a strong dehydration effect. These compounds could easily dehydrate the hydroxyl-rich EP matrix and catalyze the degradation of the matrix to form a char layer [40,41], which could well inhibit the escape of combustible gas, reduce the thermal decomposition rate, and improve the thermal stability of EP in the high-temperature stage. The T_{max2} and char residue at 700 °C of all the EP composites are higher than those of pure EP. Notably, EP/CF-PO(OPh)$_2$–10 displays lower T_{max2} and char residue at 700 °C than EP/CF-PO(OPh)$_2$–5. The heat resistance index temperature (T_{HRI}) is further calculated using the following equation [42] and listed in Table S5 The T_{HRI} decreases gradually with the increase of the CF-PO(OPh)$_2$ loading.

$$T_{HRI} = 0.49[T_{-5\%} + 0.6(T_{-30\%} - T_{-5\%})]$$

Moreover, EP composites containing CF-POPh$_2$ or CF-PPh$_2$ also show a similar phenomenon as EP/CF-PO(OPh)$_2$ composites. This is principal because of the special structure of cardanol which is composed of the

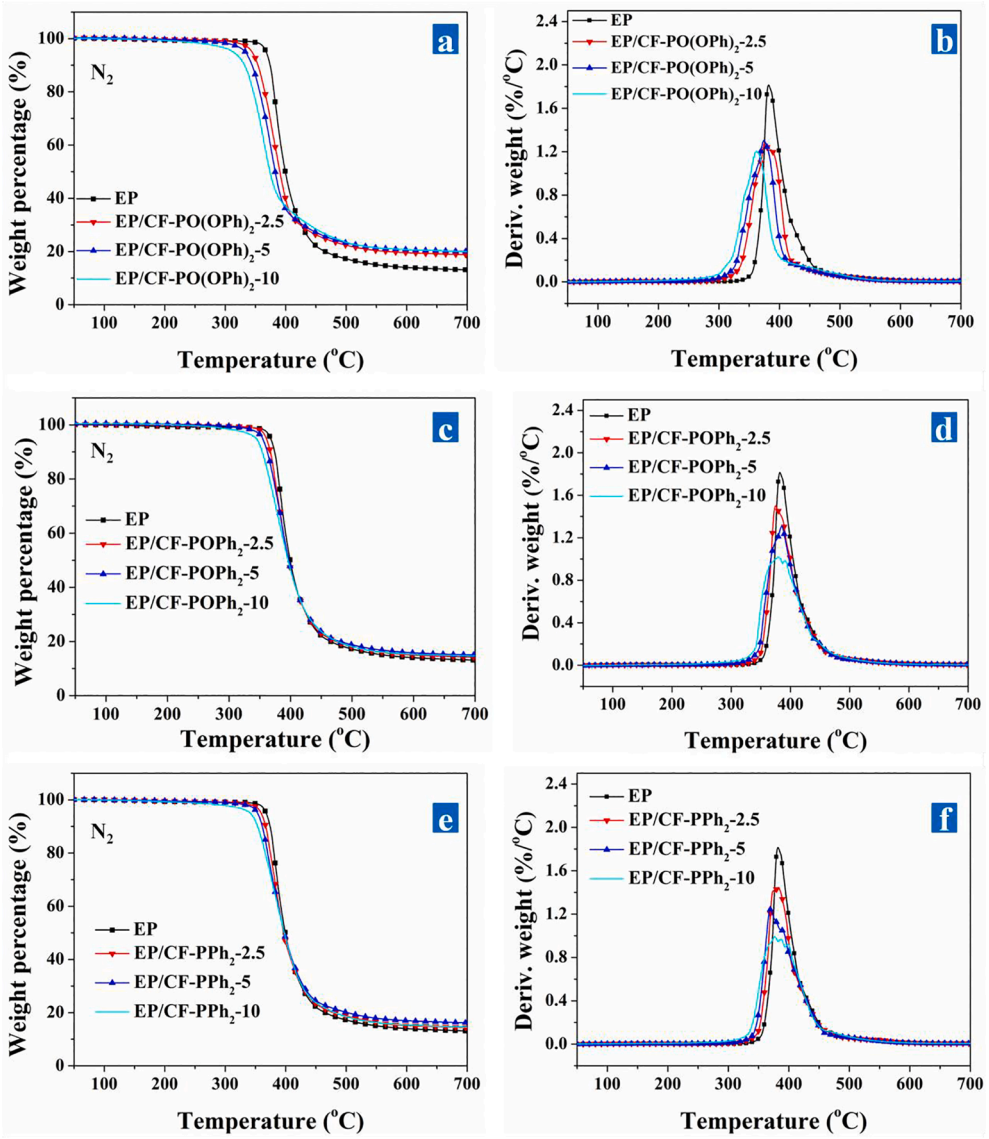

Fig. 5. TGA and DTG curves of (a, b) EP/CF-PO(OPh)$_2$, (c, d) EP/CF-POPh$_2$, and (e, f) EP/CF-PPh$_2$ composites under nitrogen atmosphere.

rigid benzene ring and flexible long aliphatic chain. In the case of lower additive amounts, the influence of benzene ring plays a leading role in the degradation process which could promote the thermal stability of the epoxy matrix; with the increasing additive amounts, the effect of the flexible long aliphatic chain becomes prominent, which could reduce the cross-linking density of the epoxy network, resulting in a slight decrease of thermal stability of EP composites, but the char yield of EP/CF-PO$(OPh)_2$–10 is still higher than that of pure EP.

The thermal degradation processes of EP and its composites under a nitrogen atmosphere were further studied. Several typical temperatures such as $T_{-5\%}$, $T_{-10\%}$, $T_{-30\%}$, T_{HRI}, and T_{max} are summarized in Table S6. As observed in Fig. 5, EP and its composites exhibit a single-stage degradation process ranging from 320 to 520 °C. Similar to the thermal-oxidative degradation process, the influence of CF-PO$(OPh)_2$, CF-$POPh_2$, and CF-PPh_2 on the thermal degradation processes of EP composites also exhibits the following behaviors including earlier degradation, catalyzing carbonization, and enhancing the char yield of EP composites. But it is worth noting that the carbonization effect of EP composites in the thermal degradation process is more significant than that of the thermal-oxidative degradation process. Taking EP/CF-PO$(OPh)_2$ composites as an example, the char residue of neat EP is about 13.1% at 700 °C, while the residual yield of EP/CF-PO$(OPh)_2$–2.5, EP/CF-PO$(OPh)_2$–5 and EP/CF-PO$(OPh)_2$–10 is improved to 18.8%, 20.1%, and 20.0%, respectively. Additionally, the residual yield of EP/CF-PO$(OPh)_2$ composites is significantly higher than that of EP/CF-$POPh_2$ and EP/CF-PPh_2 composites. This is because that the phosphate structure in CF-PO$(OPh)_2$ is apt to decompose to produce phosphoric acid compounds than CF-$POPh_2$ and CF-PPh_2, which promotes the dehydration and carbonization of the epoxy matrix to form a char layer. The formed char layer is beneficial to inhibit the escape of volatile combustible gases. Meanwhile, it can isolate the external combustion heat and oxygen from diffusing to the inside, thereby restraining further degradation of the matrix and improving the flame retardancy of epoxy composites. This conclusion would be further verified by the results of the following combustion performance tests.

DSC was then employed to study the effect of the type and content of phosphorylated cardanol-formaldehyde oligomers on the T_g, as depicted in Fig. 6. Taking CF-PO$(OPh)_2$ as an example, the T_g of pure EP is 145 °C, while EP/CF-PO$(OPh)_2$–2.5 displays a T_g of 144 °C, which is very close to that of pure EP, indicating that the introduction of a small amount of CF-PO$(OPh)_2$ slightly changes the T_g of the EP matrix; However, with increasing the addition of CF-PO$(OPh)_2$, the T_g of EP composites gradually decreases. This is mainly because that the incorporation of CF-PO$(OPh)_2$ into EP could reduce the cross-linking density of the matrix to a certain extent; moreover, the flexible long aliphatic chain in the structure of cardanol has a plasticizing effect on EP composites. Notably, the T_g values of EP/CF-PO$(OPh)_2$–10, EP/CF-$POPh_2$-10, and EP/CF-PPh_2-10 are nearly the same but all lower than that of neat EP, manifesting that all these three types of phosphorylated cardanol-formaldehyde oligomers have a plasticizing effect on EP.

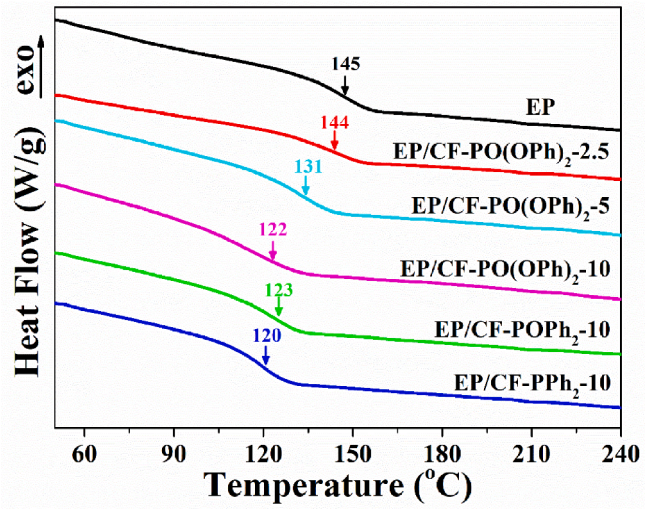

Fig. 6. DSC thermograms of epoxy composites with different types and contents of phosphorylated cardanol-formaldehyde oligomers.

3.4. Mechanical property

These three phosphorylated cardanol-formaldehyde oligomers combining rigidity and flexibility are anticipated to impart excellent mechanical property to EP composites. Typical stress–strain curves of EP and its composites are shown in Fig. 7, and the tensile strength, elastic modulus, and elongation at break are given in Table S7. It can be observed that the addition of CF-PO$(OPh)_2$, CF-$POPh_2$, and CF-PPh_2 could remarkably improve the tensile strength, tensile modulus, and elongation at break of EP composites. The pristine EP shows a tensile strength of 50.1 MPa and an elongation at break of 2.4%. For EP composites containing different contents of CF-PO$(OPh)_2$ (Fig. 7a), the tensile strength and elongation at break are enhanced, and EP/CF-PO$(OPh)_2$–5 exhibits the maximum tensile strength (68.8 MPa), which is 37.3% higher than that of EP. However, when the additive amount of CF-PO$(OPh)_2$ increased to 10 wt%, the tensile strength and tensile modulus of EP composites do not show further enhancement, but the tensile strength of EP/CF-PO$(OPh)_2$–10 (67.1 MPa) is still higher than that of neat EP and it displays the highest elongation at break (5.6%) which is raised by 133.3% as compared to pure EP. It is mainly because that CF-PO$(OPh)_2$ is composed of both rigid aromatic structure and flexible long alkane segment. In the case of low addition amount, these two structures could synergistically enhance the strength and toughness of EP composite. However, with the increase of the addition amount, the introduction of a large number of flexible segments could reduce the cross-linking density of the EP matrix [5], resulting in a decline of tensile strength and elastic modulus, but the elongation at break is steadily improved. Analogous to EP/CF-PO$(OPh)_2$ composites, the tensile strength of EP/CF-$POPh_2$ composites (Fig. 7b) displays a similar trend, and EP/CF-$POPh_2$-5 presents the maximum increment in tensile strength which is 74.2% higher than that of pure EP. Moreover, EP/CF-$POPh_2$-10 shows the most striking enhancement in elongation at break which is increased by 162.5% compared with that of pristine EP. Regarding the tensile strength of EP/CF-PPh_2 composites (Fig. 7c), the tensile strength and elongation at break of EP/CF-PPh_2-10 are 70.3 MPa and 6.0%, respectively, which are increased by 40.3% and 150.0% relative to neat EP. The above results indicate that these three phosphorylated cardanol-formaldehyde oligomers display excellent reinforcing and toughening effects. To better illustrate the toughening effect, a possible stretch-fracture model is proposed as shown in Fig. 7d. Pure EP exhibits brittleness due to its high cross-linking density, after the incorporation of phosphorylated cardanol-formaldehyde oligomers, the unique rigid-flexible structure of cardanol-based derivatives can impart excellent strength as well toughness to the epoxy matrix. Once EP composites suffer from stress, the flexible long aliphatic chain could extend firstly to transfer and absorb part of the energy during the stretching process. SEM images of the fractured sections after the tensile test have been taken for the EP/CF-PO$(OPh)_2$–10, EP/CF-$POPh_2$-10, and EP/CF-PPh_2-10 to further evaluate the reinforcing mechanism of these composites (Fig. S6 in the supplementary materials). Pristine EP displays a mirror-like fractured surface, implying its brittleness nature. By comparison, the fractured surfaces of the EP/CF-PO$(OPh)_2$–10, EP/CF-$POPh_2$-10, and EP/CF-PPh_2-10 composites become much rougher, manifesting strong interaction between CF-PO$(OPh)_2$, CF-$POPh_2$, and CF-PPh_2 with EP substrate. Additionally, there is no visible phase separation that is observed in the TEM micrographs of the EP/CF-PO$(OPh)_2$–10, EP/CF-$POPh_2$-10, and EP/CF-PPh_2-10 (Fig. S7 in the supplementary materials), indicating good compatibility of CF-PO$(OPh)_2$, CF-$POPh_2$, and CF-PPh_2

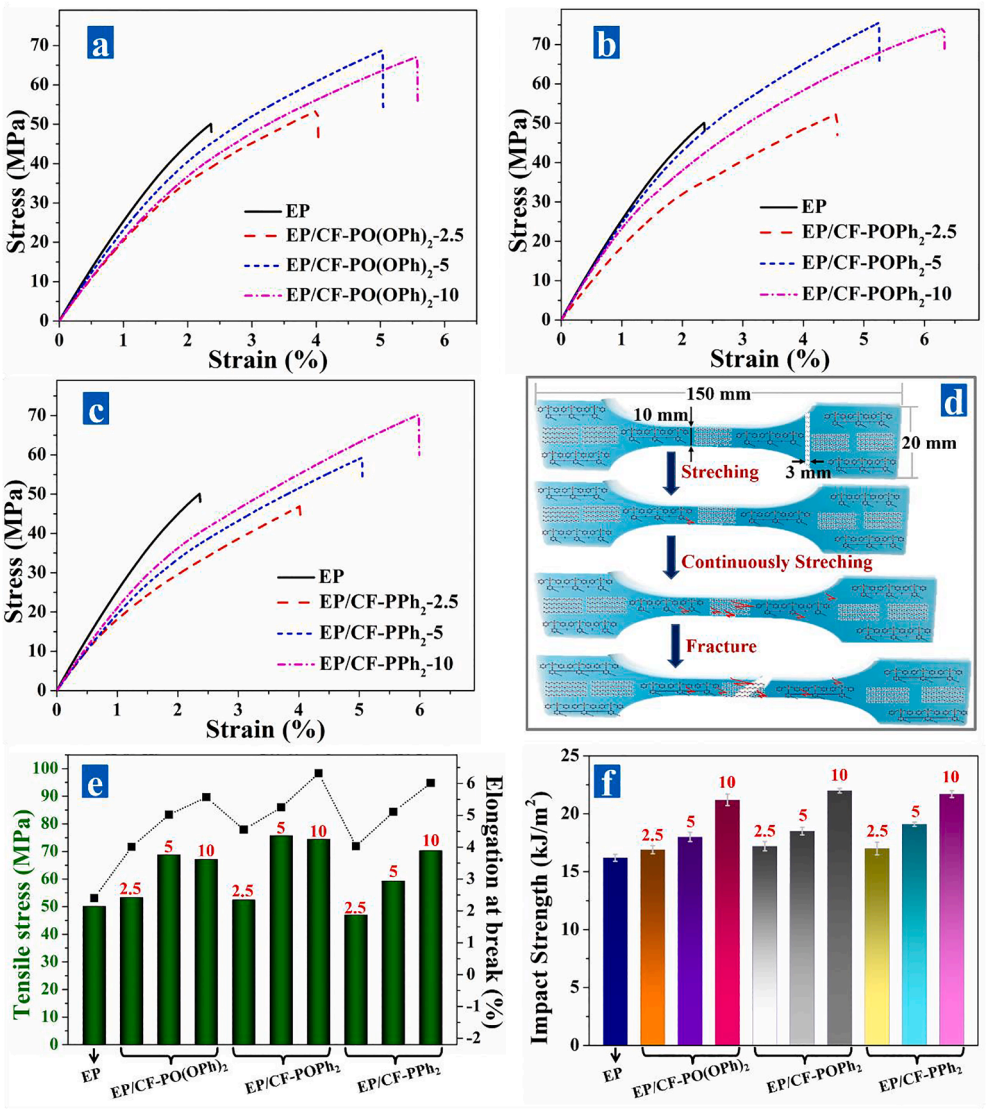

Fig. 7. Typical stress–strain curves of (a) EP/CF-PO(OPh)$_2$, (b) EP/CF-POPh$_2$ and (c) EP/CF-PPh$_2$; (d) A possible stretch-fracture model of phosphorylated cardanol-formaldehyde oligomers in epoxy composites; (e) Tensile strength and elongation at break, and (f) impact strength of EP and its composites.

in EP substrate. Since these three phosphorylated cardanol-formaldehyde oligomers have good compatibility with the EP matrix, the long side chains of phosphorylated cardanol-formaldehyde oligomers tangle with EP chains which could strengthen the matrix chains to escape from initial crack propagation. Hence, the incorporation of phosphorylated cardanol-formaldehyde oligomers can enhance mechanical property significantly (Fig. 7e).

Besides, the toughness of EP and its composites was further assessed by Izod impact tests. As depicted in Fig. 7f, the pure EP shows an impact strength of 16.2 kJ/m^2, implying intrinsic brittleness. After adding 2.5 wt% of CF-PO(OPh)$_2$, the impact strength of the epoxy composite is slightly improved to 16.9 kJ/m^2. With the increase of the amount of CF-PO(OPh)$_2$, the impact strength of EP composites is increased gradually. The maximum enhancement in the impact strength is observed in EP/CF-PO(OPh)$_2$–10, corresponding to a 30.8% increment relative to the pure EP. Moreover, the impact strength of EP composites containing CF-POPh$_2$ or CF-PPh$_2$ displays similar trends as that of EP/CF-PO(OPh)$_2$ composites. Specifically, the impact strength of EP/CF-POPh$_2$-10 and EP/CF-PPh$_2$-10 is 22.0 and 21.7 kJ/m^2, respectively. These results also demonstrate that these three phosphorylated cardanol-formaldehyde oligomers have a good toughening effect on epoxy composites. The simultaneous enhancements in the strength and toughness make EP/CF-PO(OPh)$_2$, EP/CF-POPh$_2$, and EP/CF-PPh$_2$ composites suitable for engineering applications.

3.5. Flame retardancy of EP and its composites

LOI and UL-94 tests are widespread methods to characterize the flame retardancy of materials [43]. As contrastive samples, the EP/CFR composites containing different contents (2.5, 5, and 10 wt%) of CFR were also tested by the UL-94 vertical burning method. However, all the EP/CFR composites exhibit no rating in the UL-94 vertical burning test (Fig. S8), demonstrating the poor flame-retardant effect of CFR. Thus, it is necessary to modify CFR with phosphorus-based compounds. As shown in Fig. 8, after incorporation of CF-PO(OPh)$_2$ into EP matrix, the LOI value of EP/CF-PO(OPh)$_2$–2.5 increases to 28% from 25% for pure EP. Furthermore, the LOI value is increased gradually with the increasing content of CF-PO(OPh)$_2$. EP composites containing 5 and 10 wt% of CF-PO(OPh)$_2$ exhibit higher LOI values of 30% and 32%, respectively. The other two phosphorylated cardanol-formaldehyde oligomers (CF-POPh$_2$ and CF-PPh$_2$) show a similar effect on the LOI value of EP composites, and the LOI value of EP composites containing 10% CF-POPh$_2$ and CF-PPh$_2$ is 32% and 30%, respectively, manifesting that the LOI value of EP composites is significantly improved after

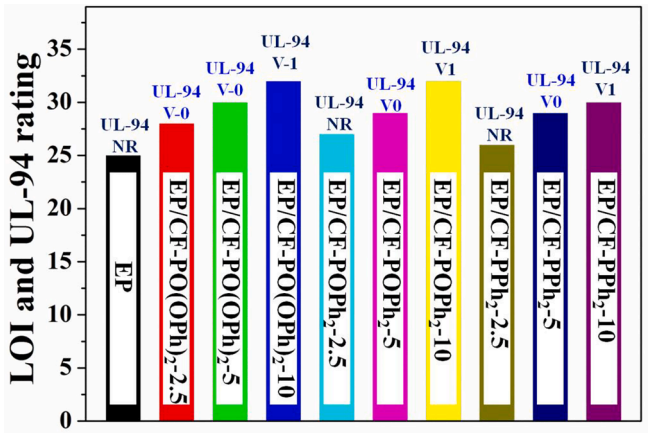

Fig. 8. LOI and UL-94 test results of EP and its composites.

incorporation of phosphorylated cardanol-formaldehyde oligomers. The UL-94 vertical burning test results are shown in Fig. 8 and the real-time images captured during the UL-94 tests of EP and EP/CF-PO(OPh)$_2$ composites are depicted in Fig. 9, in which "I" represents the first ignition and "SI" represents the second ignition; besides, the time in Fig. 9 includes the ignition time and the ignition time is 10 s each time. The flame spreads rapidly after pristine EP is ignited, and the molten dripping of EP ignites the cotton wool at the bottom (Fig. 9a). Ultimately, only a small amount of char residue is retained. For EP/CF-PO(OPh)$_2$–2.5, the flame could be quickly extinguished after twice ignitions, the total burning time after removing the ignition source is 9 s, the burning length is only 3.5 cm (Fig. 9b), manifesting that epoxy composite with only 2.5 wt% of CF-PO(OPh)$_2$ could reach UL-94 V0 rating; with the increase of CF-PO(OPh)$_2$, EP/CF-PO(OPh)$_2$–5 can still pass UL-94 V0 rating. The total burning time is shortened to 5 s, and the burning length was only 3.2 cm (Fig. 9c); Nevertheless, EP/CF-PO(OPh)$_2$–10 could only reach UL-94 V1 rating, and the total combustion time after twice ignitions is extended to 17 s (Fig. 9d). This phenomenon is mainly caused by the special structure of CF-PO(OPh)$_2$ which is composed of both phosphate structure (-PO(OPh)$_2$) and flammable long alkyl chain structure. In the case of a lower amount, the flame-retardant performance is gradually improved with the increase of the addition amount. However, when the addition amount exceeds a certain proportion, the increased amount of the flammable long alkyl chain could worsen the flame retardancy of EP composites to some extent.

Moreover, for the EP/CF-POPh$_2$ and EP/CF-PPh$_2$ composites, the real-time images captured during their combustion processes are displayed in Fig. S9. It can be observed that all the EP/CF-POPh$_2$ and EP/CF-PPh$_2$ composites could be self-extinguished without dripping during their combustion processes in the UL-94 tests, implying that CF-POPh$_2$ and CF-PPh$_2$ also have good flame-retardant property. However, epoxy composites containing 2.5 wt% of CF-POPh$_2$ or CF-PPh$_2$ have no rating in the UL-94 tests. As the content of CF-POPh$_2$ increases, EP/CF-POPh$_2$-5 could pass the UL-94 V0 rating. Further increasing the amount of CF-POPh$_2$, EP/CF-POPh$_2$-10 could only pass the UL-94 V1 rating. Besides, EP/CF-PPh$_2$-5 and EP/CF-PPh$_2$-10 also just passed the UL-94 V1 rating. Based on the results of UL-94 vertical burning tests, it can be preliminarily judged that CF-PO(OPh)$_2$ has more efficient flame-retardant performance than CF-POPh$_2$ and CF-PPh$_2$, because of a higher efficient charring ability induced by a higher phosphorus oxidation state [44].

The effect of the type and amount of phosphorylated cardanol-formaldehyde oligomers on the flame-retardant performance of epoxy composites was further evaluated by a cone calorimeter [45–47]. Fig. 10 gives the heat release rate (HRR), total heat release (THR), weight loss, and smoke production rate (SPR) versus time plots of EP and EP/CF-PO

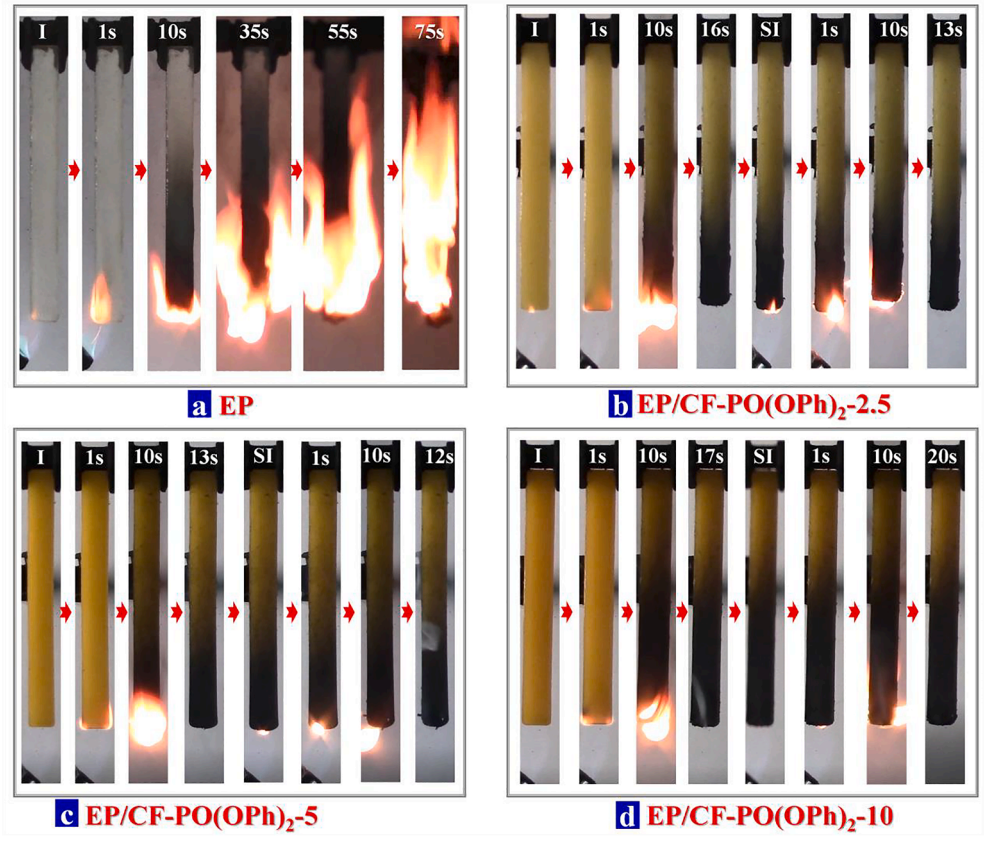

Fig. 9. The real-time images captured during the UL-94 tests of EP and EP/CF-PO(OPh)$_2$ composites.

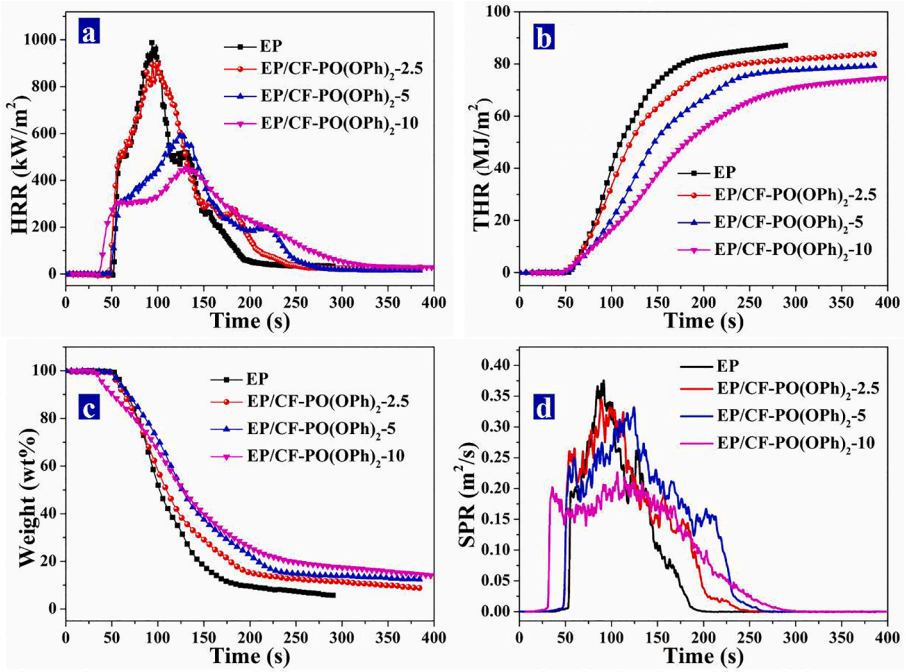

Fig. 10. The (a) heat release rate (HRR), (b) total heat release (THR), (c) weight loss, and (d) smoke production rate (SPR) versus time plots of EP and EP/CF-PO(OPh)$_2$ composites.

(OPh)$_2$ composites, and Table 2 lists the relevant data. As shown in Fig. 10a, pure EP burns violently with a time to ignition (TTI) of 50 s, showing a sharp combustion exothermic peak with an intense peak of heat release rate (PHRR) value of 985 kW/m^2. After the introduction of CF-PO(OPh)$_2$, the PHRR value of EP/CF-PO(OPh)$_2$–2.5, EP/CF-PO(OPh)$_2$–5, and EP/CF-PO(OPh)$_2$–10 composites is gradually reduced to 892, 595 and 455 kW/m^2, respectively. The maximum PHRR reduction of up to 53.8% is observed for EP/CF-PO(OPh)$_2$–10 composite. In Fig. 10b, all the THR curves show a similar upward trend with the extension of radiation time and gradually becomes flat as burning ends. The THR value of pure EP is 87.1 MJ/m^2. The THR value of EP composites gradually decreases with the increase of CF-PO(OPh)$_2$ content. Notably, the THR reduction of EP/CF-PO(OPh)$_2$–2.5, EP/CF-PO(OPh)$_2$–5, and EP/CF-PO(OPh)$_2$–10 is approximately 4.6%, 9.2%, and 13.8%, respectively, as compared to that of pristine EP. From the weight loss curve (Fig. 10c), it can be observed that with the increase of CF-PO(OPh)$_2$ addition, the weight loss rate of EP/CF-PO(OPh)$_2$ composites during the combustion process is lower than that of pure EP, and the final char yield of EP/CF-PO(OPh)$_2$–2.5, EP/CF-PO(OPh)$_2$–5 and EP/CF-PO(OPh)$_2$–10 is significantly improved to 8.6%, 12.2%, and 14.0%, respectively, from 5.7% for neat EP. This phenomenon accords well with the results of TGA tests which is mainly due to the excellent charring ability of CF-PO(OPh)$_2$ with a higher phosphorus oxidation state. The formed char layer can block the escape of internal combustible gases and the supply of external heat and oxygen, thereby inhibiting further combustion of epoxy matrix and enhancing the fire safety of EP composites. Besides the heat-related parameters, smoke is an important non-heat factor for flame-retardant materials. From Fig. 10d, it can be observed that a large amount of smoke is emitted during the combustion process of pristine EP, owing to its rich aromatic structures. With increasing the addition of CF-PO(OPh)$_2$, the peak smoke production rate of EP/CF-PO(OPh)$_2$ composites gradually decreases, which is attributed to the excellent char-forming capacity of EP/CF-PO(OPh)$_2$ composites. The formed dense char layer has a good physical barrier effect, which can suppress the escape of volatile smoke and flammable products generated by the degradation of the internal matrix, thereby suppressing the smoke release rate.

As shown in Table 2, with the increase of CF-PO(OPh)$_2$ content, the TTI value of EP/CF-PO(OPh)$_2$ is lowered gradually while the T_{PHRR} shifts to a higher zone. This is mainly ascribed to the superior catalytic carbonization effect of CF-PO(OPh)$_2$: in the early stage of combustion, CF-PO(OPh)$_2$ first decomposes to produce strongly dehydrated phosphoric acid compounds, which could catalyze the dehydration of the matrix into char. Consequently, the TTI of all the EP/CF-PO(OPh)$_2$ composites becomes earlier than pure EP, which is well consistent with the TGA results; More importantly, the thermal degradation of the matrix in advance could form a stable phosphorous-containing protective char layer which could be beneficial to inhibiting heat and mass transfer and suppressing flame spread. As a result, the T_{PHRR}s of EP/CF-PO(OPh)$_2$ composites are delayed gradually. Moreover, the fire growth rate index (FIGRA) is another important index for evaluating the fire propensity of polymeric materials, which is obtained through dividing PHRR by time to PHRR (T_{PHRR}). The lower the FIGRA value, the higher the fire safety of polymer materials [48]. After the incorporation of CF-

Table 2
Cone calorimeter data of EP and its composites.

Sample	TTI (s)	T_{PHRR} (s)	PHRR (kW/m^2)	THR (MJ/m^2)	Reduction in PHRR (%)	FIGRA (kW/ (m^2·s))	Char yield (%)
EP	50	95	985	87.1	–	10.4	5.7
EP/CF-PO(OPh)$_2$–2.5	47	100	892	83.9	9.4	8.9	8.6
EP/CF-PO(OPh)$_2$–5	48	123	595	79.3	39.6	4.8	12.2
EP/CF-PO(OPh)$_2$–10	37	134	455	75.0	53.8	3.4	14.0
EP/CF-POPh$_2$-10	42	98	769	77.5	21.9	7.8	6.4
EP/CF-PPh$_2$-10	43	109	818	79.4	17	7.5	6.6

$PO(OPh)_2$, the FIGRA value of EP/CF-$PO(OPh)_2$ is reduced significantly. The maximum reduction of FIGRA is observed for EP/CF-$PO(OPh)_2$–10, which is 67.3% lower than that of pure EP, indicating the significantly reduced fire risk of EP/CF-$PO(OPh)_2$ composites. Based on the above results, it can be speculated that the introduction of CF-$PO(OPh)_2$ into the EP matrix significantly inhibits the heat and smoke release rates, reduces the flame spread rate, and consequently improves the fire safety of epoxy composites.

Besides, the influence of the phosphorylated cardanol-formaldehyde oligomers on the fire risk features of epoxy composites is also studied by cone calorimeter. Fig. S10 shows the HRR, THR, weight loss, and SPR versus time plots of EP and EP composites containing three types of phosphorylated cardanol-formaldehyde oligomers. Compared with pure EP, the PHRR value of EP/CF-$PO(OPh)_2$–10, EP/CF-$POPh_2$-10, and EP/CF-PPh_2-10 is decreased by 53.8%, 21.9%, and 17.0%, respectively (Fig. S10a). From the THR curves (Fig. S10b), it can be found that the THR curves of EP/CF-$PO(OPh)_2$–10, EP/CF-$POPh_2$-10, and EP/CF-PPh_2-10 all show an obvious backward trend, indicating that these three phosphorylated cardanol-formaldehyde oligomers can well inhibit the rapid heat release of the epoxy matrix. The THR reduction sequence of these three flame retardant epoxy composites is as follows: EP/CF-$PO(OPh)_2$–10 (13.9%) > EP/CF-$POPh_2$-10 (11.0%) > EP/CF-PPh_2-10 (8.8%). Based on the PHRR and THR reduction results, it can be found that CF-$PO(OPh)_2$ exhibits better flame-retardant efficiency than CF-$POPh_2$ and CF-PPh_2. This is mainly attributed to the phosphate structure in CF-$PO(OPh)_2$, which is more conducive to generate phosphoric acid compounds that could better catalyze the carbonization of the EP matrix to form a stable protective char layer. Compared to CF-$PO(OPh)_2$, there are fewer oxygen atoms connected to phosphorus in the structure of CF-$POPh_2$, and phosphorus is only connected to carbon atoms in the structure of CF-PPh_2. Therefore, these two phosphorylated cardanol-formaldehyde oligomers cannot produce phosphoric acid during thermal decomposition, leading to their inferior catalytic charring ability. This conclusion could be supported by the weight loss curve during combustion processes (Fig. S10c). The char yield follows the order of EP/CF-$PO(OPh)_2$–10 (14.0%) > EP/CF-$POPh_2$-10 (6.4%) ≈ EP/CF-PPh_2-10 (6.6%) > EP (5.7%), indicating the best charring ability of CF-$PO(OPh)_2$. Fig. S10d shows the SPR curves of EP composites with three phosphorylated cardanol-formaldehyde oligomers. It can be observed that the peak SPR value of EP/CF-$PO(OPh)_2$–10 is significantly decreased compared to that of pure EP, while the SPR value of EP/CF-$POPh_2$-10 and EP/CF-PPh_2-10 do not display obvious reduction. Based on the above results, it can be inferred that all these three phosphorylated cardanol-formaldehyde oligomers can improve the flame-retardant performance of epoxy composites, and CF-$PO(OPh)_2$ exhibits the best flame-retardant efficiency among them since the phosphate structure in CF-$PO(OPh)_2$ possesses superior charring ability.

Based on the results aforementioned, the flame-retardant efficiency of phosphorylated cardanol-formaldehyde oligomers is compared with the reported flame-retardant toughening agents, as shown in Table S8. It can be observed that the EP/CF-$PO(OPh)_2$–5 could achieve the UL-94 V0 rating with only a 5 wt% flame-retardant toughening agent, which exhibits better efficiency than most of the reported flame-retardant toughening agents [2,5,6,49–51]. Besides, the reduction in PHRR for the EP/CF-$PO(OPh)_2$–5 achieves 39.6% at a relatively low loading of the flame-retardant toughening agent. The higher flame-retardant efficiency of the EP/CF-$PO(OPh)_2$–5 could be attributed to the unique oligomeric structure and phosphorus-containing group.

3.6. Flame-retardant mechanism analysis

Fig. 11. shows the digital photos of char residues from both top and side views for EP and its composites after cone calorimeter tests. There is only a very small amount of char residue left after the violent combustion of pure EP (Fig. 11a). With the increased amount of CF-$PO(OPh)_2$, the remaining amount of char residues of EP composites increases significantly. It can be observed from the top view that as the amount of CF-$PO(OPh)_2$ increases, the surface morphology of the char layer for EP/CF-$PO(OPh)_2$ composites gradually changes from fluffy and porous to dense and intact. Moreover, it can also be discovered from the side-view

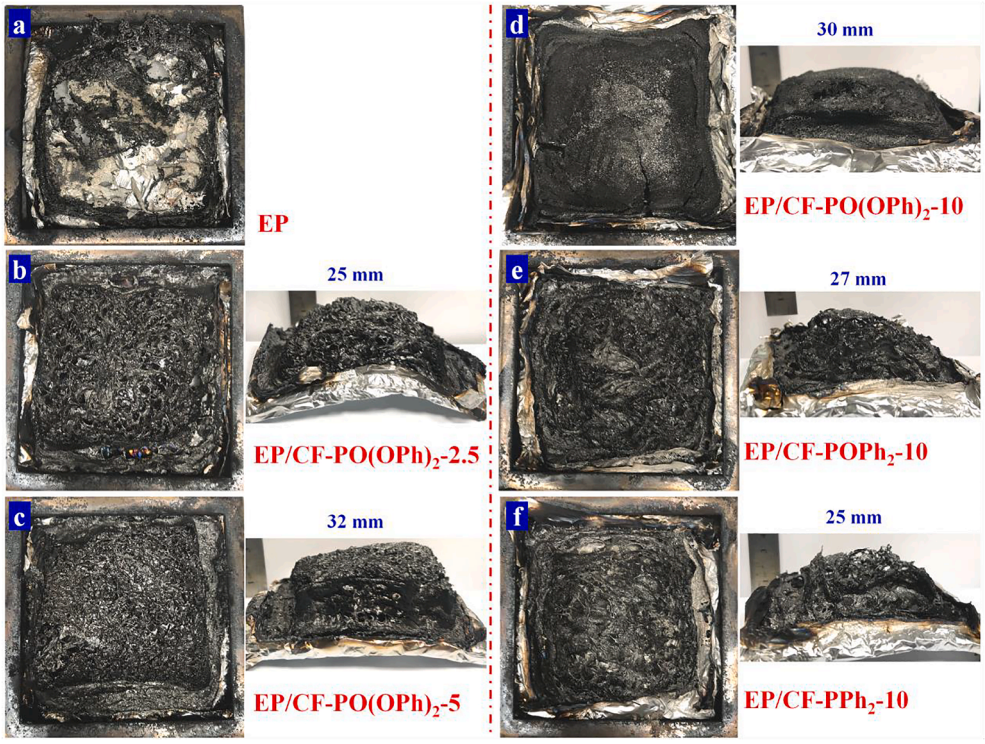

Fig. 11. Digital photos of the char residues from both top and side views for (a) EP, (b) EP/CF-$PO(OPh)_2$–2.5, (c) EP/CF-$PO(OPh)_2$–5, (d) EP/CF-$PO(OPh)_2$–10, (e) EP/CF-$POPh_2$-10 and (f) EP/CF-PPh_2-10 after the cone calorimeter test.

photos that EP/CF-PO(OPh)$_2$ composites show excellent charring ability, and the thickness of the char layer increases gradually with increasing the content of CF-PO(OPh)$_2$. Notably, EP/CF-PO(OPh)$_2$–10 (Fig. 11d) exhibits the densest char layer among all EP composites, indicating that the char layer of EP/CF-PO(OPh)$_2$–10 has the best barrier effect, which is well consistent with the analysis results of the cone calorimeter test. By comparing the char residues of EP composites with 10 wt% three phosphorylated cardanol-formaldehyde oligomers, it is found that the char layers of EP/CF-POPh$_2$-10 (Fig. 11e) and EP/CF-PPh$_2$-10 (Fig. 11f) not only present a loose and porous structure but also have a poorer intumescence as compared with that of EP/CF-PO(OPh)$_2$–10, implying that CF-PO(OPh)$_2$ has a superior catalytic carbonization effect over CF-POPh$_2$ and CF-PPh$_2$, which can significantly improve the char formation ability of EP composites.

SEM was further employed to study the char morphology of EP and its composites. As shown in Fig. S11a, there are many cracks and large open pores in the char of pure EP, which cannot hinder the permeation of oxygen into the inner and accelerate fire propagation. By contrast, the cracks and holes on the surface of the chars of EP/CF-PO(OPh)$_2$–2.5 (Fig. S11b), EP/CF-PO(OPh)$_2$–5 (Fig. S11c), and EP/CF-PO(OPh)$_2$–10 (Fig. S11d) are decreased gradually, and the char surface of EP/CF-PO(OPh)$_2$–10 becomes more compact and denser. This featured surface morphology is ascribed to the higher charring ability and the less release of volatile gases. However, the char surfaces of EP/CF-POPh$_2$-10 (Fig. S11e) and EP/CF-PPh$_2$-10 (Fig. S11f) have some small holes which are not so tight and dense as that of EP/CF-PO(OPh)$_2$–10. The char layer with compact and thick morphology is favorable to retard the heat and mass transfer, thus could effectively suppress the degradation and protect the underlying materials.

The graphitization degree performs a great important role in reducing the fire risk of polymers, and the higher graphitization degree indicates higher thermal resistance and greater protective effect [48,52–54]. Raman spectroscopy is one of the most commonly employed tools to study the graphitization degree of residual chars after combustion. The Raman spectra of the char residues of EP and its composites are shown in Fig. S12. It can be found that all the samples display two prominent peaks at around 1364 and 1596 cm^{-1}, corresponding to the D and G bands, respectively. The intensity ratio of the D to G band (I_D/I_G) is usually applied to evaluate the graphitization degree of the char residues [48,55]. The lower I_D/I_G means a higher graphitization degree. The I_D/I_G of pure EP is about 3.10, and the I_D/I_G of EP/CF-PO(OPh)$_2$ composite shows a gradually decreasing trend with the increased addition of CF-PO(OPh)$_2$, implying that CF-PO(OPh)$_2$ has a positive effect on improving the graphitization degree of residual chars of EP composites. Besides, the I_D/I_G value of EP/CF-POPh$_2$-10 (2.94) and EP/CF-PPh$_2$-10 (2.92) is higher than that of EP/CF-PO(OPh)$_2$–10 (2.59), indicating that the char residue of EP/CF-PO(OPh)$_2$–10 has a higher graphitization degree, namely higher thermal stability and better shielding effect, which is beneficial to enhance the fire safety of EP composites.

Based on the degradation and combustion behaviors analysis aforementioned, a possible flame-retardant mechanism of EP composites containing CF-PO(OPh)$_2$, CF-POPh$_2$ and CF-PPh$_2$ is proposed in Fig. 12. Generally, phosphorus-based flame-retardants function in both condensed and gaseous phase mechanisms. As reported previously, the catalytic charring ability improved and the emission of PO· radicals decreased as the phosphorus oxidation states increased [44]. Once exposed to heat and fire sources, CF-PO(OPh)$_2$ could decompose to generate phosphoric acid species, which can catalyze the degradation of the EP matrix to form a compact and intumescent char layer. The more compact and intumescent char layer is beneficial to inhibiting heat and mass transfer and suppressing the release of volatile flammable products to feed the flame. Compared to CF-PO(OPh)$_2$, there are fewer oxygen atoms connected to phosphorus in the structure of CF-POPh$_2$, and phosphorus is only connected to carbon atoms in the structure of CF-PPh$_2$. Thus, the CF-POPh$_2$ and CF-PPh$_2$ cannot decompose to produce phosphoric acid species, resulting in poorer catalytic charring ability. Besides, the flame-retardant effect relates closely with the char yield for the epoxy composites with different loadings of the phosphorylated cardanol-formaldehyde oligomer. The EP/CF-PO(OPh)$_2$–10, EP/CF-

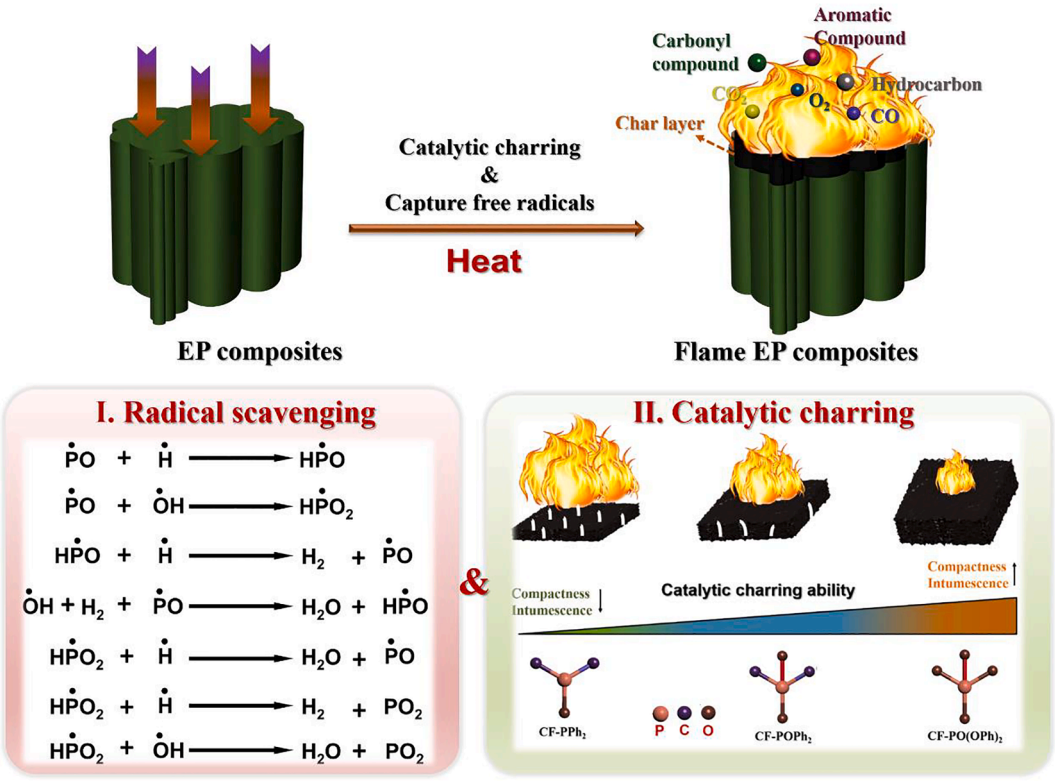

Fig. 12. A possible flame-retardant mechanism of EP composites containing phosphorylated cardanol-formaldehyde oligomers.

$POPh_2$-10, and EP/CF-PPh_2-10 show poorer flame-retardant property in terms of UL-94 than the EP/CF-$PO(OPh)_2$–5, EP/CF-$POPh_2$-5, and EP/CF-PPh_2-5, because the former samples possess lower char yield. Thus, the EP composites with CF-$PO(OPh)_2$ exhibit the highest efficient fire safety characteristics, implying that the catalytic charring ability plays a predominant role over the radical scavenging effect in these three phosphorylated cardanol-formaldehyde oligomers.

4. Conclusions

In this work, three kinds of phosphorylated cardanol-formaldehyde oligomers (CF-$PO(OPh)_2$, CF-$POPh_2$, and CF-PPh_2) were synthesized and introduced into epoxy thermosets. Comparison of the effect of CF-$PO(OPh)_2$, CF-$POPh_2$, and CF-PPh_2 on the mechanical, thermal, and flame-retardant properties of the epoxy thermosets was investigated. The incorporation of CF-$PO(OPh)_2$, CF-$POPh_2$, and CF-PPh_2 showed toughening effect on the EP composites in terms of the increased impact strength and elongation at break, owing to the presence of flexible long alkyl chain structure. EP composites containing CF-$PO(OPh)_2$, CF-$POPh_2$, and CF-PPh_2 also exhibited enhanced flame-retardant behavior. Among them, CF-$PO(OPh)_2$ exhibited the highest flame-retardant efficiency, because of the superior catalytic charring effect over CF-$POPh_2$ and CF-PPh_2. Specifically, epoxy composite with only 2.5 wt% CF-$PO(OPh)_2$ could pass the UL-94 V-0 rating as well as a high LOI value of 28%, and the LOI value of EP/CF-$PO(OPh)_2$–10 reached up to 32%. Cone calorimeter tests indicated that EP composite containing 10 wt% CF-$PO(OPh)_2$ exhibited a significant PHRR reduction up to 53.8% compared to pure EP. This work demonstrates cardanol can serve as a promising platform for the synthesis of bio-based flame-retardant and toughening agents combining rigidity with flexibility and contributes to the production of high-performance epoxy thermosets.

Declaration of Competing Interest

The authors declare that they have no known competing financial interests or personal relationships that could have appeared to influence the work reported in this paper.

Acknowledgments

We gratefully acknowledge financial support from the Natural Science Foundation of China (No. 22075265) and the Fundamental Research Funds for the Central Universities (No.: WK2320000047).

Appendix A. Supplementary data

Supplementary data to this article can be found online at https://doi.org/10.1016/j.cej.2021.130192.

References

[1] Z.B. Shao, M.X. Zhang, Y. Li, Y. Han, L. Ren, C. Deng, A novel multi-functional polymeric curing agent: Synthesis, characterization, and its epoxy resin with simultaneous excellent flame retardance and transparency, Chem. Eng. J. 345 (2018) 471–482.
[2] W. Guo, X. Wang, C.S.R. Gangireddy, J. Wang, Y. Pan, W. Xing, L. Song, Y. Hu, Cardanol derived benzoxazine in combination with boron-doped graphene toward simultaneously improved toughening and flame retardant epoxy composites, Compos. Part A-Appl. S. 116 (2019) 13–23.
[3] X. Wang, Y. Hu, L. Song, W. Xing, H. Lu, P. Lv, G. Jie, Flame retardancy and thermal degradation mechanism of epoxy resin composites based on a DOPO substituted organophosphorus oligomer, Polymer 51 (2010) 2435–2445.
[4] J.H. Zhang, X.Q. Mi, S.Y. Chen, Z.J. Xu, D.H. Zhang, M.H. Miao, J.S. Wang, A bio-based hyperbranched flame retardant for epoxy resins, Chem. Eng. J. 381 (2020), 122719.
[5] X. Wang, S. Zhou, W.-W. Guo, P.-L. Wang, W. Xing, L. Song, Y. Hu, Renewable cardanol-based phosphate as a flame retardant toughening agent for epoxy resins, ACS Sustain. Chem. Eng. 5 (2017) 3409–3416.
[6] F.K. Chu, C. Ma, T. Zhang, Z.M. Xu, X.W. Mu, W. Cai, X. Zhou, S.C. Ma, Y.F. Zhou, W.Z. Hu, L. Song, Renewable vanillin-based flame retardant toughening agent with ultra-low phosphorus loading for the fabrication of high-performance epoxy thermoset, Compos. Part B-Eng. 190 (2020), 107925.
[7] Y. Ma, H.H. Di, Z.X. Yu, L. Liang, L. Lv, Y. Pan, Y.Y. Zhang, D. Yin, Fabrication of silica-decorated graphene oxide nanohybrids and the properties of composite epoxy coatings research, Appl. Surf. Sci. 360 (2016) 936–945.
[8] Z.G. Xu, P.G. Song, J. Zhang, Q.P. Guo, Y.W. Mai, Epoxy nanocomposites simultaneously strengthened and toughened by hybridization with graphene oxide and block ionomer, Compos. Sci. Technol. 168 (2018) 363–370.
[9] B.H. Yuan, Y.R. Sun, X.F. Chen, Y.Q. Shi, H.M. Dai, S. He, Poorly-/well-dispersed graphene: Abnormal influence on flammability and fire behavior of intumescent flame retardant, Compos. Part A-Appl. S. 109 (2018) 345–354.
[10] B.B. Chen, Y.H. Jia, M.J. Zhang, H.Y. Liang, X. Li, J. Yang, F.Y. Yan, C.S. Li, Tribological properties of epoxy lubricating composite coatings reinforced with core-shell structure of CNF/MoS_2 hybrid, Compos. Part A-Appl. S. 122 (2019) 85–95.
[11] C.M. Vu, Q.V. Bach, L.X. Duong, N.V. Thai, V.D. Thao, P.T. Duc, D.D. Nguyen, T. Hoang, T.N. Van, Silane coupling agent with amine group grafted nano/micro-glass fiber as novel toughener for epoxy resin: fabrication and mechanical properties, Compos. Interface 20 (2020) 1–16.
[12] A. Bahrami, F. Cordenier, P. Van Velthem, W. Ballout, T. Pardoen, B. Nysten, C. Bailly, Synergistic local toughening of high performance epoxy-matrix composites using blended block copolymer-thermoplastic thin films, Compos. Part A-Appl. S. 91 (2016) 398–405.
[13] F. Xu, X.S. Du, H.Y. Liu, W.G. Guo, Y.W. Mai, Temperature effect on nano-rubber toughening in epoxy and epoxy/carbon fiber laminated composites, Compos. Part B-Eng. 95 (2016) 423–432.
[14] L.H. Xiao, J.R. Huang, Y.G. Wang, J. Chen, Z.S. Liu, X.A. Nie, Tung oil-based modifier toughening epoxy resin by sacrificial bonds, ACS Sustain. Chem. Eng. 7 (2019) 17344–17353.
[15] H.B. Gu, H.Y. Zhang, C. Ma, X.J. Xu, Y.Q. Wang, Z.C. Wang, R.B. Wei, H. Liu, C. T. Liu, Q. Shao, X.M. Mai, Z.H. Guo, Trace electrosprayed nanopolystyrene facilitated dispersion of multiwalled carbon nanotubes: Simultaneously strengthening and toughening epoxy, Carbon 142 (2019) 131–140.
[16] S.Z. Haeri, M. Asghari, B. Ramezanzadeh, Enhancement of the mechanical properties of an epoxy composite through inclusion of graphene oxide nanosheets functionalized with silica nanoparticles through one and two steps sol-gel routes, Prog. Org. Coat. 111 (2017) 1–12.
[17] X.M. Fei, F.Q. Zhao, W. Wei, J. Luo, M.Q. Chen, X.Y. Liu, Tannic Acid as a Bio-Based Modifier of Epoxy/Anhydride Thermosets, Polymers 8 (2016) 314.
[18] P.Y. Jia, M. Zhang, C.G. Liu, L.H. Hu, G.D. Feng, C.Y. Bo, Y.H. Zhou, Effect of chlorinated phosphate ester based on castor oil on thermal degradation of poly (vinyl chloride) blends and its flame retardant mechanism as secondary plasticizer, RSC Adv. 5 (2015) 41169–41178.
[19] T. Liu, L.C. Sun, R.X. Ou, Q. Fan, L.P. Li, C.G. Guo, Z.Z. Liu, Q.W. Wang, Flame retardant eugenol-based thiol-ene polymer networks with high mechanical strength and transparency, Chem. Eng. J. 368 (2019) 359–368.
[20] W. Xie, S. Huang, D. Tang, S. Liu, J. Zhao, Biomass-derived Schiff base compound enabled fire-safe epoxy thermoset with excellent mechanical properties and high glass transition temperature, Chem. Eng. J. 123667 (2019).
[21] Y. Qi, Z.H. Weng, K.W. Zhang, J.Y. Wang, S.H. Zhang, C. Liu, X.G. Jian, Magnolol-based bio-epoxy resin with acceptable glass transition temperature, processability and flame retardancy, Chem. Eng. J. 387 (2020), 124115.
[22] Y. Qi, Z. Weng, Y. Kou, L. Song, J. Li, J. Wang, S. Zhang, C. Liu, X. Jian, Synthesize and introduce bio-based aromatic s-triazine in epoxy resin: Enabling extremely high thermal stability, mechanical properties, and flame retardancy to achieve high-performance sustainable polymers, Chem. Eng. J. 406 (2021), 126881.
[23] T.K.L. Nguyen, S. Livi, B.G. Soares, G.M.O. Barra, J.F. Gerard, J. Duchet-Rumeau, Development of Sustainable Thermosets from Cardanol-based Epoxy Prepolymer and Ionic Liquids, ACS Sustain. Chem. Eng. 5 (2017) 8429–8438.
[24] C.Y. Bo, L.H. Hu, P.Y. Jia, B.C. Liang, J. Zhou, Y.H. Zhou, Structure and thermal properties of phosphorus-containing polyol synthesized from cardanol, RSC Adv. 5 (2015) 106651–106660.
[25] P. Jia, F. Song, Q. Li, H. Xia, M. Li, X. Shu, Y. Zhou, Recent Development of Cardanol Based Polymer Materials-A Review, J. Renew. Mater. 7 (2019) 601–619.
[26] K. Wazarkar, A. Sabnis, Synthesis and Characterization of UV Oligomer based on Cardanol, J. Renew. Mater. 8 (2020) 57–68.
[27] R.S. Gour, V.V. Kodgire, M.V. Badiger, Toughening of epoxy novolac resin using cardanol based flexibilizers, J. Appl. Polym. Sci. 133 (2016) 43318.
[28] W. Guo, B. Yu, Y. Yuan, L. Song, Y. Hu, In situ preparation of reduced graphene oxide/DOPO-based phosphonamidate hybrids towards high-performance epoxy nanocomposites, Compos. Part B: Eng. 123 (2017) 154–164.
[29] B. Yu, W. Xing, W. Guo, S. Qiu, X. Wang, S. Lo, Y. Hu, Thermal exfoliation of hexagonal boron nitride for effective enhancements on thermal stability, flame retardancy and smoke suppression of epoxy resin nanocomposites via sol-gel process, J. Mater. Chem. A 4 (2016) 7330–7340.
[30] M. Natarajan, S.C. Murugavel, Synthesis, spectral and thermal degradation kinetics of novolac resins derived from cardanol, High Perform. Polym. 25 (2013) 685–696.
[31] Z.S. Liu, J. Chen, G. Knothe, X.A. Nie, J.C. Jiang, Synthesis of Epoxidized Cardanol and Its Antioxidative Properties for Vegetable Oils and Biodiesel, ACS Sustain. Chem. Eng. 4 (2016) 901–906.
[32] G. Phalak, D. Patil, A. Patil, S. Mhaske, Synthesis of acrylated cardanol diphenyl phosphate for UV curable flame-retardant coating application, Eur. Polym. J. 121 (2019), 109320.
[33] X.Y. Li, X. Nie, J. Chen, Y.G. Wang, Preparation of epoxidized cardanol butyl ether as a novel renewable plasticizer and its application for poly(vinyl chloride), Polym. Int. 66 (2017) 443–449.

[34] R. Shukla, P. Kumar, Self-curable epoxide resins based on cardanol for use in surface coatings, Pigm. Resin Technol. 40 (2011) 311–333.
[35] M. Natarajan, S.C. Murugavel, Cure kinetics of bio-based epoxy resin developed from epoxidized cardanol-formaldehyde and diglycidyl ether of bisphenol-A networks, J. Therm. Anal. Calorim. 125 (2016) 387–396.
[36] C. Ma, S.L. Qiu, J.L. Wang, H.B. Sheng, Y. Zhang, W.Z. Hu, Y. Hu, Facile synthesis of a novel hyperbranched poly(urethane-phosphine oxide) as an effective modifier for epoxy resin, Polym. Degrad. Stabil. 154 (2018) 157–169.
[37] Y. Fu, W.H. Zhong, Cure kinetics behavior of a functionalized graphitic nanofiber modified epoxy resin, Thermochim. Acta 516 (2011) 58–63.
[38] X. Wang, Y. Hu, L. Song, W. Xing, H. Lu, Thermal degradation mechanism of flame retarded epoxy resins with a DOPO-substitued organophosphorus oligomer by TG-FTIR and DP-MS, J. Anal. Appl. Pyrol. 92 (2011) 164–170.
[39] W. Cai, Z. Li, X. Mu, L. He, X. Zhou, W. Guo, L. Song, Y. Hu, Barrier function of graphene for suppressing the smoke toxicity of polymer/black phosphorous nanocomposites with mechanism change, J. Hazard. Mater. 404 (2021), 124106.
[40] C. Ma, B. Yu, N. Hong, Y. Pan, W. Hu, Y. Hu, Facile synthesis of a highly efficient, halogen-free, and intumescent flame retardant for epoxy resins: Thermal properties, combustion behaviors, and flame-retardant mechanisms, Ind. Eng. Chem. Res. 55 (2016) 10868–10879.
[41] C. Ma, S.L. Qiu, B. Yu, J.L. Wang, C.M. Wang, W.R. Zeng, Y. Hu, Economical and environment-friendly synthesis of a novel hyperbranched poly (aminomethylphosphine oxide-amine) as co-curing agent for simultaneous improvement of fire safety, glass transition temperature and toughness of epoxy resins, Chem. Eng. J. 322 (2017) 618–631.
[42] A. Satdive, S. Mestry, P. Borse, S. Mhaske, Phosphorus- and silicon-containing amino curing agent for epoxy resin, Iran. Polym. J. 29 (2020) 433–443.
[43] Y. Zhang, W.X. Tian, L.X. Liu, W.H. Cheng, W. Wang, K.M. Liew, B.B. Wang, Y. Hu, Eco-friendly flame retardant and electromagnetic interference shielding cotton fabrics with multi-layered coatings, Chem. Eng. J. 372 (2019) 1077–1090.
[44] M.M. Velencoso, A. Battig, J.C. Markwart, B. Schartel, F.R. Wurm, Molecular firefighting-how modern phosphorus chemistry can help solve the challenge of flame retardancy, Angew. Chem. Int. Edit. 57 (2018) 10450–10467.
[45] W. Cai, Y. Hu, Y. Pan, X. Zhou, F. Chu, L. Han, X. Mu, Z. Zhuang, X. Wang, W. Xing, Self-assembly followed by radical polymerization of ionic liquid for interfacial engineering of black phosphorus nanosheets: Enhancing flame retardancy, toxic gas suppression and mechanical performance of polyurethane, J. Colloid Interf. Sci. 561 (2019) 32–45.
[46] D. Wang, X. Feng, L. Zhang, M. Li, M. Liu, A. Tian, S. Fu, Cyclotriphosphazene-bridged periodic mesoporous organosilica-integrated cellulose nanofiber anisotropic foam with highly flame-retardant and thermally insulating properties, Chem. Eng. J. 375 (2019), 121933.
[47] J.L. Wang, C. Ma, X.W. Mu, X. Zhou, L.X. He, Y.L. Xiao, L. Song, Y. Hu, Designing 3D ternary-structure based on SnO_2 nanoparticles anchored hollow polypyrrole microspheres interconnected with N, S co-doped graphene towards high-performance polymer composite, Chem. Eng. J. 402 (2020), 126221.
[48] W. Guo, X. Wang, J. Huang, Y. Zhou, W. Cai, J. Wang, L. Song, Y. Hu, Construction of durable flame-retardant and robust superhydrophobic coatings on cotton fabrics for water-oil separation application, Chem. Eng. J. 398 (2020), 125661.
[49] Y. Qiu, L. Qian, H. Feng, S. Jin, J. Hao, Toughening Effect and Flame-retardant behaviors of phosphaphenanthrene/phenylsiloxane bigroup macromolecules in epoxy thermoset, Macromolecules 51 (2018) 9992–10002.
[50] C. Zhao, D. He, Y. Wang, Y. Xing, Y. Li, Flame retardant and toughening mechanisms of core–shell microspheres, RSC Adv. 5 (2015) 85329–85337.
[51] W.A. Wei, L.A. Yuan, W.B. Hui, W.A. Qi, Synthesis of a hyperbranched polyamide charring agent and its flame-retarding and toughening behavior in epoxy resin, Polym. Degrad. Stabil. 184 (2021), 109479.
[52] D. Wang, H. Peng, B. Yu, K. Zhou, H. Pan, L. Zhang, M. Li, M. Liu, A. Tian, S. Fu, Biomimetic structural cellulose nanofiber aerogels with exceptional mechanical, flame-retardant and thermal-insulating properties, Chem. Eng. J. 389 (2020), 124449.
[53] D. Wang, H. Peng, Y. Wu, L. Zhang, M. Li, M. Liu, Y. Zhu, A. Tian, S. Fu, Bioinspired lamellar barriers for significantly improving the flame-retardant properties of nanocellulose composites, ACS Sustain. Chem. Eng. 8 (2020) 4331–4336.
[54] B. Yuan, Y. Hu, X. Chen, Y. Shi, Y. Niu, Y. Zhang, S. He, H. Dai, Dual modification of graphene by polymeric flame retardant and $Ni(OH)_2$ nanosheets for improving flame retardancy of polypropylene, Compos. Part A-Appl. S. 100 (2017) 106–117.
[55] Z. Xu, W. Xing, Y. Hou, B. Zou, L. Han, W. Hu, Y. Hu, The combustion and pyrolysis process of flame-retardant polystyrene/cobalt-based metal organic frameworks (MOF) nanocomposite, Combust. Flame 226 (2021) 108–116.